Pyrak-Nolte ,L.J. & Nolte, D.D., 2025, Role of intersections in fracture connectivity,
Accepted for Publication Nov 4, 2025 in the Journal of Geophysical Research: Solid Earth, 130, e2025JB033007,
https://doi.org/10.1029/2025JB033007

Role of Intersections in Fracture Connectivity

L. J. Pyrak-Nolte[1,2,3*] and D. D. Nolte[1]

[1]Department of Physics & Astronomy, Purdue University, Lafayette, Indiana.

[2]Department of Earth, Atmospheric & Planetary Sciences, Purdue University, Lafayette, Indiana.

[3]Lyles School of Civil Engineering, Purdue University, Lafayette, Indiana.

*Corresponding author: Laura J. Pyrak-Nolte (ljpn@purdue.edu)

†Additional author notes should be indicated with symbols (current addresses, for example).

Key Points:

- The contribution of intersections to fracture network connectivity depends on the stress-dependent spatial correlations in fracture aperture distributions.
- Intersections enhance connectivity in flow directions parallel to intersections.
- Corners cause correlated clusters on one fracture to be disconnected from correlated clusters on the other fracture, reducing the connectivity of a network.

Abstract

Networks of intersecting fractures often provide the flow paths through subsurface reservoirs. Assessing network connectivity is challenging because fracture intersections compose a vanishingly small fraction of the network void volume. In this paper, motivated by 3D X-ray imaging of the simplest element of fracture network, i.e., two orthogonal fractures, we perform a percolation and finite-size scaling analysis to study the connectivity provided by fracture intersections. The conditions when an intersection enhances connectivity across a sample depend on spatial correlations in the fracture aperture distributions, on the stress state, and on the direction of flow. Here we consider three flow directions: (1) across intersections, (2) parallel to intersections and (3) around corners. For (1), intersections provide minimal enhancement of connectivity because they contribute little additional void area. For (2), intersections increase the probability of a connected path near threshold by enabling 3D connected pathways that are not possible in parallel fractures. Flow around corners, (3), is fundamentally the result of the intersection connecting two fractures in series and spatial correlations are broken around corners, suppressing the connectivity relative to (1). When the connected fractures are stressed equally, a joint percolation threshold emerges that continues to have scale invariance. However, when the fractures are stressed unequally, the system has mixed percolation without clearly-defined percolation thresholds. In all cases, percolation probabilities are found to be scale dependent which has important consequences for the connectivity of larger fracture networks composed of the fundamental element studied here.

Plain Language Summary

Fractures in rocks in the Earth control many properties of importance to human activity, such as the stability of tunnels and the ability to extract or store fluids underground. Single fractures may be limited in size, but networks of fractures can extend over long distances, enhancing the flow of fluids, for instance in enhanced geothermal systems or in hydrocarbon reservoirs. The intersection between two fractures is a fundamental element in such fracture networks, and understanding the fluid transport properties at such an intersection provides the foundation upon which broader understanding of fracture networks is built. In this paper, using X-ray tomography, we measure the geometric properties of fracture intersections under stress. Based on these results, we use percolation theory to predict how the connectivity of fluid paths along or across intersections are affected by changing stress conditions. We find that while intersections play little role for transport directly across the fracture intersection, the intersection plays a dominant role in fluid transport that crosses from one fracture to another (around corners). Furthermore, the geometric properties of the fractures play an important role determining how strong these effects are. Understanding the percolation properties of fracture intersections provides the first step towards understanding the broader properties of fracture networks.

Index Terms—Fractures, fracture networks, percolation

1 Introduction

Natural and induced fracture networks are often the key pathways for the injection and withdrawal of fluids in energy-related applications. For example, the 2017 DOE Basic Research Needs report on "*Energy and Water*"(Tirrell et al., 2017) recognized that overcoming the dual challenges of maximizing the lifetime of a geothermal reservoir, while minimizing water usage, required a fundamental understanding of how to create, maintain and manage a fracture network. Control and manipulation of fracture networks is also important for traditional and unconventional oil and gas resources and for subsurface water resource development, as well as for subsurface storage projects (CO_2, H_2). These applications cause complex interactions that perturb (physically, thermally, and chemically) fracture network connectivity over the lifetime of a project. Consequently, an improved understanding of what affects and contributes to fracture connectivity is required to sustain subsurface activities.

Understanding connectivity of a fracture network begins by defining the topological elements that form a network. Topological elements are often defined from 2D views from outcrops, tunnels or boreholes. Although fracture networks are intrinsically 3D, these 2D sections enable one to infer the topological elements of a system (Bai et al., 2000; S.E. Laubach et al., 2019; Peacock et al., 2018; D.J. Sanderson & Nixon, 2015). The simplest topological elements of fracture networks are often referred to "X", "Y or T" and "V" (Figure 1) based on the shape of the intersecting fractures (Stephen E Laubach et al., 2018; S.E. Laubach et al., 2019; Peacock et al., 2018; D.J. Sanderson & Nixon, 2015; David J Sanderson & Nixon, 2018). These simple topological elements are composed of two intersecting fractures sharing one intersection. Although there is an extended hierarchy of topological elements in a fracture network, it is important to understand how the base elements of these simplest topological elements (i.e., single fractures and intersections) affect fracture network connectivity.

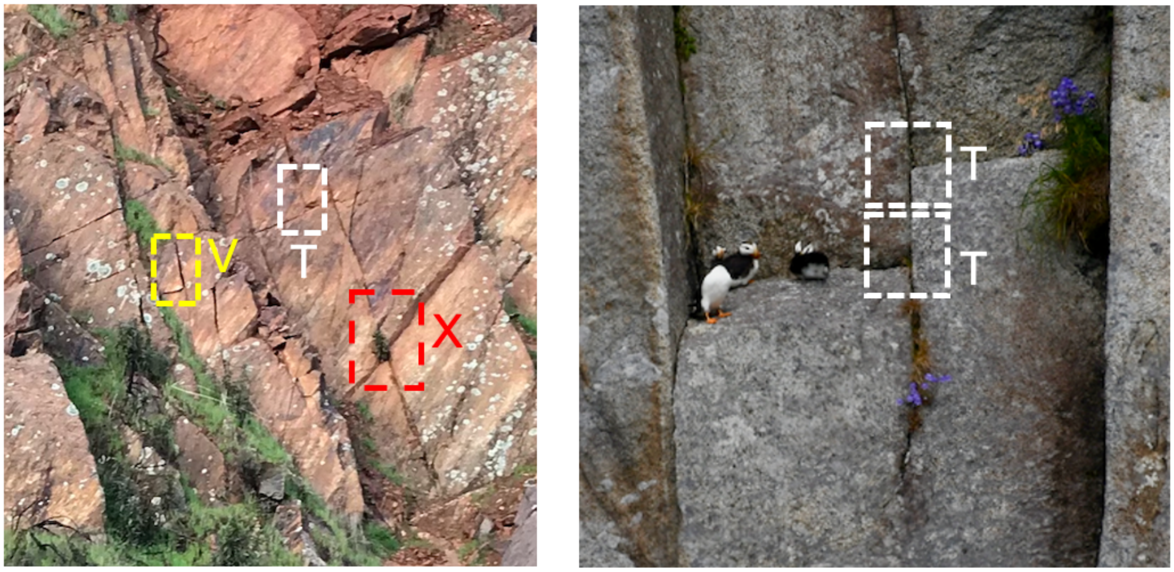

Figure 1. (left) Rock outcrop with “X”, “T” and “V” topological elements from California Route 120 on cut-off to the Old Priest Grade, Priest, California. (right) “T” topological element in rock outcrop on Granite Island in Kenai Fjords National Park, Alaska with puffins for scale.

For single fractures, the literature is rich in studies that show that the void geometry in a fracture controls the flow path geometry and connectivity along the fracture plane as a function of stress(Berkowitz, 2002; Boutt et al., 2006; Brown et al., 1998; Council, 1996; Deng et al., 2024; Durham & Bonner, 1995; He et al., 2025; Nemoto et al., 2009; D. D. Nolte, Pyrak-Nolte, L. J., and Cook, N. G. W., 1989; Pyrak-Nolte et al., 1988; Raven & Gale, 1985; C. F. Tsang & Neretnieks, 1998; Y. W. Tsang & Tsang, 1987; Viswanathan et al., 2022; Welch et al., 2021; Witherspoon et al., 1980; Wood, 2024). The hydraulic, mechanical and seismic responses of single fractures were shown to be linked by the fracture void geometry (Petrovitch et al., 2014; Pyrak-Nolte, 2019; Pyrak-Nolte & Nolte, 2016) which includes spatial correlations as well as the probability distribution functions of apertures and contact areas between two rough surfaces in contact. As this geometry deforms under stress, the contact area between the two surfaces increases, the voids deform, and the flow path geometry and connectivity within single fractures are altered. With stress, a fracture can transition from an effective medium region, where there are multiple parallel flow paths across a fracture, to a percolation regime where connectivity is controlled by only a few flow paths (Petrovitch et al., 2014; Pyrak-Nolte, 2019; Pyrak-Nolte & Nolte, 2016). A single fracture under sufficiently high stress may cease to support fluid flow and transmit seismic waves as if it were a welded contact (i.e. "intact" material) (Pyrak-Nolte et al., 1990).

Fracture intersections are also base elements of fracture networks, providing the connectivity that enables long-range transport over distances larger than the average length of any single fracture in the network. The role of fracture intersections in the evolution of fracture network connectivity has been largely overlooked, yet without intersections, fractures would be isolated in space. The behavior of intersections is central to how a network evolves in response to changing physical and chemical processes. Closure or sealing of an intersection can radically affect the geometry of the transport paths that provide access to fracture surfaces in a system. In contrast to the wealth of studies on single fractures, considerably fewer experimental studies have been performed on fracture networks and their flow properties and how they deform under stress (e.g.(Asahina et al., 2014; Frash et al., 2017; Frash et al., 2016; Frash et al., 2019; Hull & Koslow, 1986; Johnson & Brown, 2001; Johnson et al., 2006; Montemagno & Pyrak-Nolte, 1999; Stockman et al., 2001; Viswanathan et al., 2022)). 3D discrete fracture network simulations with different aperture distributions in each fracture (Frampton et al., 2019) observed discontinuities in permeability between intersecting fractures which affected flow channeling and the travel-times/residence-times of solutes transported through a network. Connectivity was improved by enhancing the intersection permeability which led to notable decreases in residence times, but raises questions of what the geometry of a fracture intersection is under stress and how it affects mixing rules used for solute transport through fracture networks.

Stanton-Yonge et al. (Stanton-Yonge et al., 2023) performed hydrostatic tests on a rock core with 2 induced intersecting fractures with an "X" topology to compare the permeability to a core with 2 induced parallel fractures. From optical microscopy on 2D thin sections from the core, the intersection was found to be irregular in shape with apertures larger than the adjacent fractures. The core with an "X" topology was found to be more permeable than two parallel non-intersecting fractures. The flow measurements were taken along the intersection which can act as a short circuit between the inlet and outlet, suggesting that the intersection remained open and connected under stress. Another study (Santos et al., 2022) used 3D X-ray tomography to image the change in an "X" topological element as a function of stress and observed that whether an intersection remained open or closed depended on the spatial correlations in the aperture distributions and on the orientation of the "X" topological element relative to an applied uni-axial stress field. These studies raise many questions: do two intersecting fractures always support more flow than 2 parallel fractures?; How does stress affect the connectivity among the base elements of a network?; How does connectivity changes with scale of observation?; and How is connectivity around corners affected by the aperture distributions of the individual fracture planes?

Here, a percolation and finite-size scaling analysis is performed to address these questions. Percolation and finite-size scaling analysis (Stauffer, 1987) is a sophisticated yet simple tool for assessing connectivity of void space in a fracture network, yielding not only the probability of whether there is a connected path across a fracture or a fracture network but also providing information on how this connectivity scales with the length scale of observation. Figure 2 shows an example of the spanning probability P(A,L) as a function of void area fraction for a single fracture with a random distribution of apertures for observation length scales of 1/32, 1/16, 1/8, ¼, ½ and 1 (arbitrary units). At the critical area fraction, A_c, the spanning probability, $P(A_c)$, is scale invariant, i.e. all observation scales have the same probability of having a connect path across the

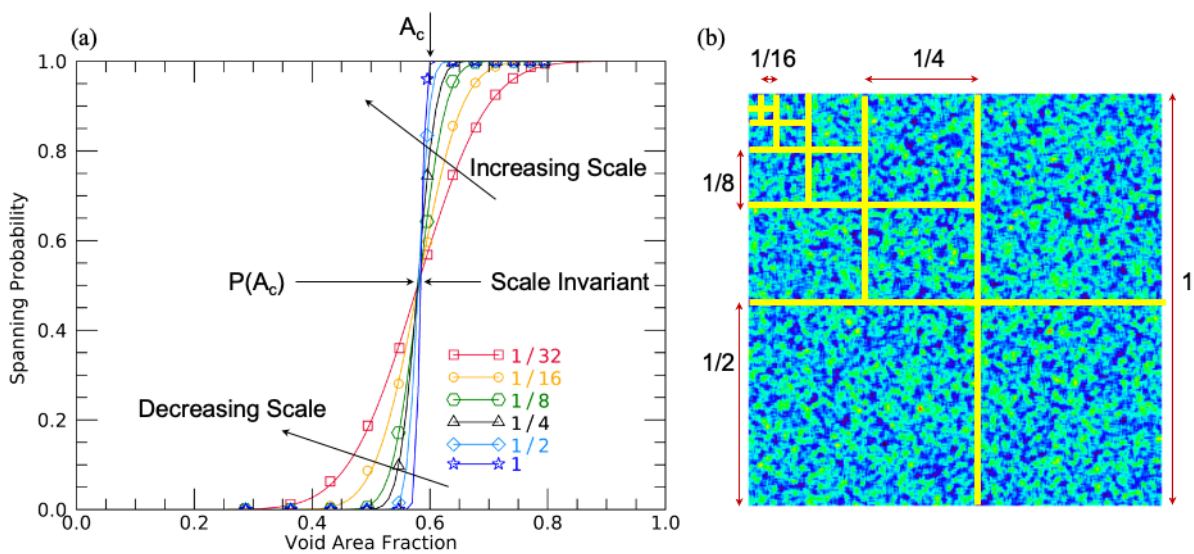

Figure 2. (a) Single-fracture spanning probability, *P(A,L)*, as a function of area fraction, *A*, for different observation scales. A_c is the critical area fraction where the spanning probability, $P(A_c)$ is scale invariant. (*right*) Sub-sectioning of a single fracture into 1/32, 1/16, 1/8, ¼, ½ of the original length, *L* =1, for a random aperture distribution (blue – green – yellow – red increasing aperture) used to perform finite-size analysis as a function of scale. Note: 1/32 size is not shown in (b).

fracture. Below the fixed point, *P(L)* decreases with an increase in observation scale L, and conversely, above the fixed point, *P(L)* increases with increasing observation scale. Thus the magnitude of the probability of having a connected path depends on the scale of observation, except at the threshold A_c. These concepts will be applied to understanding the spanning probability (i.e. connectivity) across an "X" topological element under stress.

Percolation approaches have previously been used to study the connectivity in single fractures with aperture distributions (e.g.(D. D. Nolte, and Pyrak-Nolte, L. J., 1997; D. D. Nolte & Pyrak-Nolte, 1991; Petrovitch et al., 2014)), in 2D fracture networks with fractures having different but constant aperture (e.g. (J.-R. de Dreuzy et al., 2001; Ye et al., 2021)) and 3D networks with length and shape distributions but with each fracture having a constant aperture (e.g.(Hamzehpour et al., 2021; Mourzenko et al., 2005; David J Sanderson & Nixon, 2018; Thovert et al., 2017)). De Dreuzy et al. (J. R. de Dreuzy et al., 2012) performed a Monte Carlo study using a discrete fracture network (DFN) model to study flow through 3D fracture networks. The networks consisted of random fractures with different lengths (and in turn variable-length intersections) and each fracture had an aperture distribution. They noted that the location of an intersection in a fracture, either through a large void or an area contact (or low transmissivity), had a strong impact on flow, flow channeling and disconnection of flow paths. While the simulation of a full network provided interesting results, a more fundamental study is needed on just a single topological element to fully understand the role of the probabilistic and spatial distribution of apertures on the intersection geometry and on connectivity, considering how this is influenced by stress, and how connectivity can extend into 3D depending on the spatial correlations in the aperture distributions.

In this paper, we present 3D X-ray tomographic reconstructions of "X" topological elements to demonstrate the changes in the geometry with stress. Laboratory data were collected for two stress cases: (1) when the "X" topological element had an "x" orientation relative to an applied normal stress, causing both fractures to close under stress; and (2) when the "X" topological element had a "+" orientation relative to an applied normal stress, causing a reduction in apertures on the horizontal fracture while the vertical fracture was unaffected by stress. Motivated by these experimental observations, a Monte Carlo study is performed to examine the effect of spatial correlations on the spanning probability across the intersection (referred to as left-to-right, LR), in a direction parallel to the intersection (front-to-back, FB) and around corners (Northwest, NW). The FB spanning probabilities are compared to the spanning probabilities for two parallel independent (non-intersecting) fractures to determine if the observations from Stanton-Yonge et al.(Stanton-Yonge et al., 2023) hold for different stress conditions, aperture distributions and scales of observation. For the percolation analysis, the "x" orientation is in a "homogeneous percolation regime" because the spatial correlations and reduction in apertures from stress are the same in both fractures, similar to lithostatic conditions in the subsurface (assuming no deviatoric stresses). However, the "+" orientation is in a "mixed percolation regime" because only one fracture is changing with stress. The "+" orientation is similar to the stress conditions in regions with tectonic extension or uniaxial-strain reference state where the vertical load can be greater than the lateral confinement (vertical stress > lateral stresses). From our analysis, we show that stress condition, void area fractions and spatial correlations in the fracture aperture distribution determine under what conditions, and by how much, fracture intersections affect the connectivity of fracture networks and when scaling is applicable.

2 Experimental Observations

The motivation for the percolation study is based on results from 3D tomographic imaging of a simple network under stress. Although there is an extended hierarchy of topological elements in natural fracture networks, the "X" topological element is taken as the focus of this paper to aid in understanding how this most basic element of network topology changes under stress. In this section, we describe the experimental approach and the results from analyzing the volumetric reconstructions of the fracture intersection.

1.1 Experimental Approach

1.1.1 Sample Fabrication

A simple fracture network was designed based on an "X" network topology that is composed of two intersecting orthogonal fractures. The samples were constructed from 3D printed prisms of an acrylate-based polymer (Figure 3a&b). An "x" orientation of the "X" topology experiences equal stresses on both fracture planes under normal loading (Figure 3f). A "+" orientation (Figure 3e) was used to preferentially load the horizontal fracture. For the "x" orientation, the network was assembled from four 3D printed triangular prisms (~ 3 x 6 x 6 mm^3 each) that had surface roughness on the rectangular lateral faces but not on the base (Figure 3a). For the "+" orientation, the sample was composed of four 3D printed rectangular prisms (~ 3 x 3 6 mm^3 each) with roughness on two sides (Figure 3b). The surface roughness was designed with either random (samples: +Random & xRandom) or spatially correlated (samples: +Correlated and xCorrelated) asperity distributions that were generated using a stratified percolation approach (D. D. Nolte & Pyrak-Nolte, 1991) (see Section 3 for a description of the pattern generation and Table 1 for parameters used to generate the patterns). Opposing fracture surfaces were mirror images of each

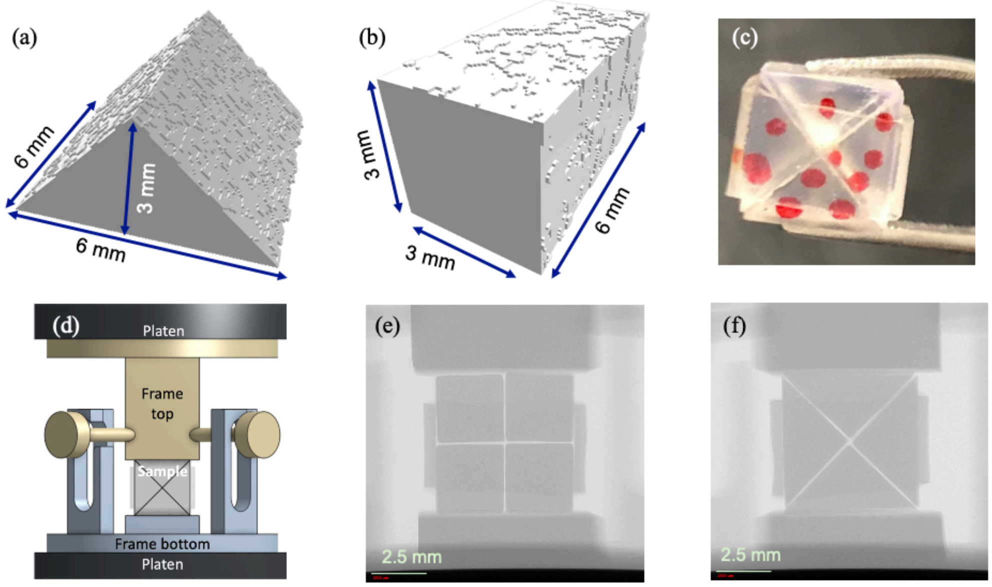

Figure 3. Sample fabrication and testing. Examples of computer generated stl files used for 3D printing (a) a triangular prism and (b) rectangular prism to create topological networks with different orientations for loading. (c) Image of an "x" orientation network fabricated from (a) triangular prisms. (d) Drawing of a sample in the loading system with alignment guides. 2D X-ray images of (e) "+" and (f) "x" orientations relative to loading for an X topological network.

other, i.e. not mated. The blocks were printed with photopolymer clear resin on a Formlabs 3 printer with a layer thickness of 25 micrometers (Figure 3c). Printed blocks were cleaned in a 5-minute isopropyl alcohol wash followed by a 2-minute drip dry, which was repeated 3 times, or until no excess resin remained. The cleaned blocks were then cured in a UV LED light chamber set to 35◦C for 20 minutes.

1.1.2 3D X-ray Tomographic Imaging Under Stress

Heat shrink tubing (light gray outside the sample in Figure 3e&f) was shrunk onto the perimeter of the sample to provided lateral confinement. The sample was placed into a 3D printed

https://doi.org/10.1029/2025JB033007

custom frame (same printing materials and parameters as the sample) to control sample alignment during set-up and loading (Figure 3d). The frame with mounted sample was placed inside a Deben CT5000 stress rig inside a Zeiss Versa 510 3D X-ray microscope to acquire 2D X-ray projections of the sample that were then used for 3D volumetric tomographic reconstructions of the fracture network geometry. The frame was designed to prevent significant slip along the fractures by having loading platens that are larger than the sample width. The load was applied with a displacement rate of 0.1 mm/minute. 3D X-ray volumetric imaging was performed for several selected normal loads (25, 100 and 200 N) 30 minutes after reaching the desired load to allow the system to equilibrate. The settings for the X-ray imaging were 80 kV at 7 Watts, 0.4x magnification, bin 2, 3.5 sec exposure time, 2401 projections, and source and detector distances of 73 and 334 mm, respectively. This yielded a voxel edge length of 12.3 micrometers.

1.2 Visualization and Analysis of 3D Fracture Network Geometry

3D tomographic reconstructions of the fracture networks enable the examination of stress effects on the network void volume, contact area and intersection geometry. Figure 4 shows the reconstructed network for a "+" orientation relative to loading for a random (Figure 4a-c) and a spatially correlated (Figure 4d-g) asperity distributions. The aperture distributions in Figure 4

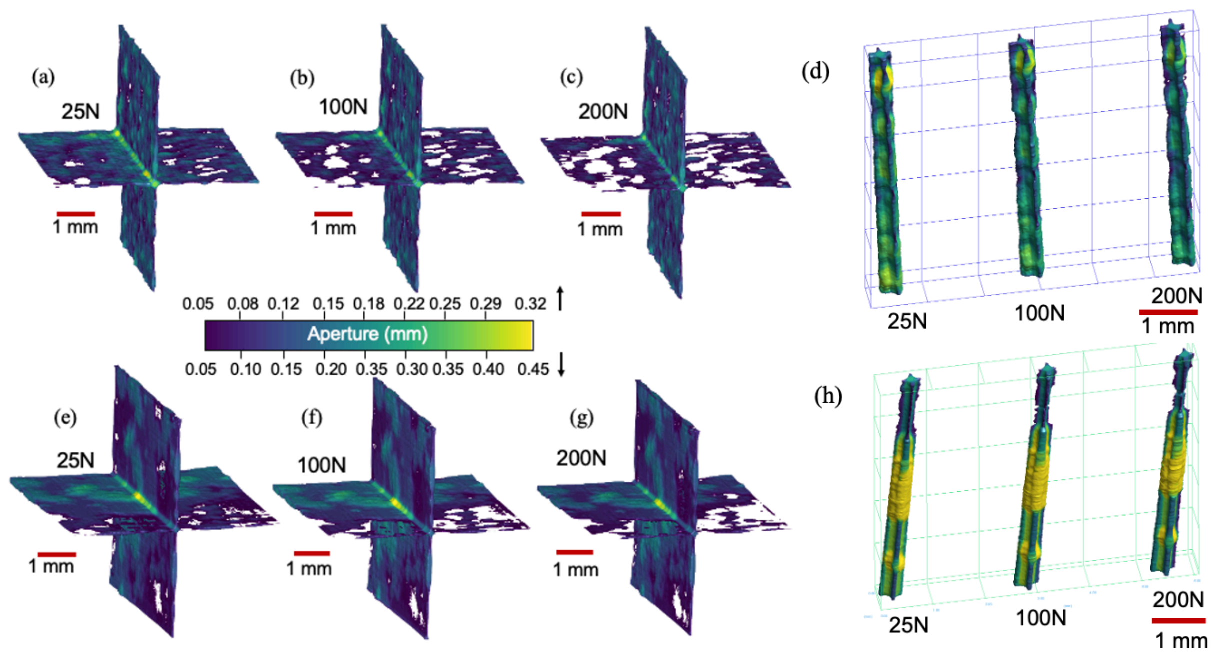

Figure 4. 3D reconstruction of aperture distribution for the X topological network in the "+" orientation for (a-c) samples +Random and (e-g) +Correlated for normal loads of 25, 100 and 200N. Intersection geometry is shown for the "+" orientation for (d) random and (h) spatially correlated asperity distribution for normal loads of 25, 100 and 200N. The color scale gives the aperture in millimeters. The scale represents 1 mm.

were obtain from the thickness mapping function in the DragonFly™ reconstruction software that uses a Laplace smoothing function. White regions in the figures are contact area but may also be apertures of less than one voxel. The intersection geometry (Figures 3d&f) was extracted from the networks using custom codes written in IDL and then visualized using the same thickness mapping function in DragonFly™. For the "+" orientation, only the apertures in the horizontal fracture are significantly affected by increasing the load from 25 N to 200 N (Figures 4a-c,e-g). The vertical fracture is approximately unaffected, and the intersection remains connected with increasing load (Figures 4d&h). As the load on the sample is increased, the two intersecting fractures change to have differing void area fractions and contact areas (white regions in Figures 4a-c & *5a*-c) which leads to a mixed percolation regime. The differences in the void geometry

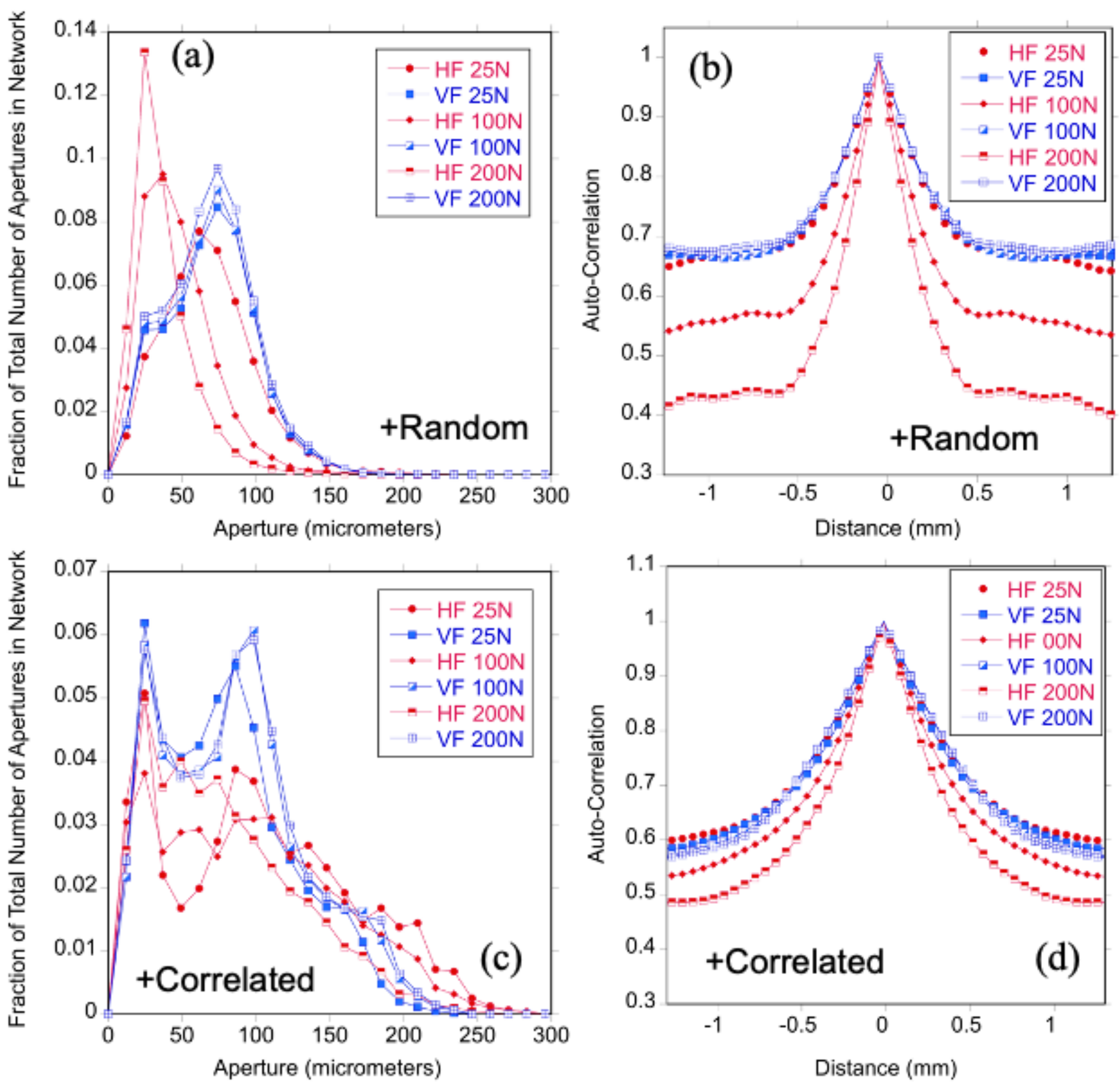

Figure *5*. (a&c) Aperture distributions and (b&d) auto-correlation functions for samples +Random and +Correlated for normal loads of 25, 100 and 200 N. HF – horizontal fracture, VF – vertical fracture.

between the vertical and horizontal fracture with increasing load is captured by the changes in the aperture distributions and spatial correlations that occur (Figure 5). The aperture distributions (Figure 5a&c) show that the probability distribution for the horizontal fracture shifts to lower values of apertures with increasing load while for the vertical fracture, the aperture distribution remains relatively constant. An auto-correlation analysis (Figure *5b*) shows that the spatial correlations (Figures 5b&d) in the vertical fracture are unaffected by stress. However, the spatial correlation length of the horizontal fracture decreases with increasing load.

When the fracture network is in the "x" orientation ((Figures 6&7), both fractures are subjected to similar normal and shear stresses, unlike the fractures in the "+" orientation. These similar stresses result in a reduction in aperture for both fractures in the network (Figure 7a&c). An auto-correlation analysis for the "x" orientation (Figures 7b&d) shows that the spatial correlations do not change significantly, and the correlation length remains unchanged with increasing load. As the load increases from 25 N to 100 N, the intersection becomes weakly connected, and then at

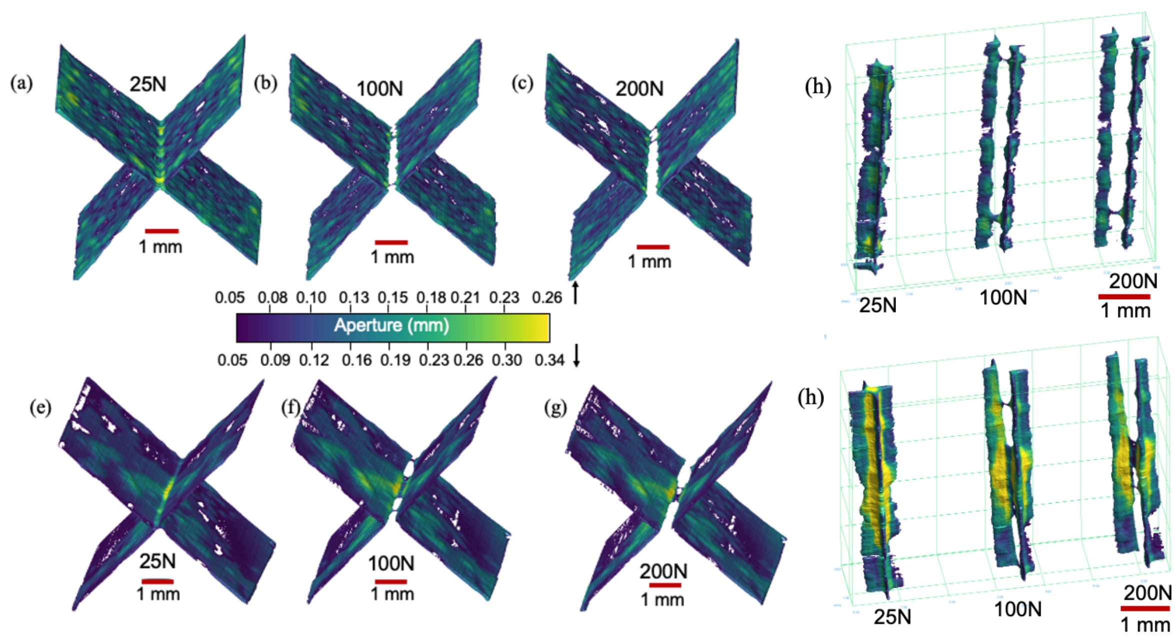

Figure 6. 3D reconstruction of aperture distribution for samples (a-c) xRandom and (e-g) xCorrelated for normal loads of 25, 100 and 200N. Intersection geometry is shown "x" orientation for (d) random and (h) spatially correlated asperity distribution for normal loads of 25, 100 and 200N. The color scale gives the aperture in millimeters. The scale represents 1 mm.

200 N almost completely disconnects (Figures 6h). The topology of the network transitions from a "X" to two disconnected "V" topological elements, each with their own intersection. The effect

of the spatial correlations in the original asperity distribution is reflected in the spatial distribution of apertures and contact area.

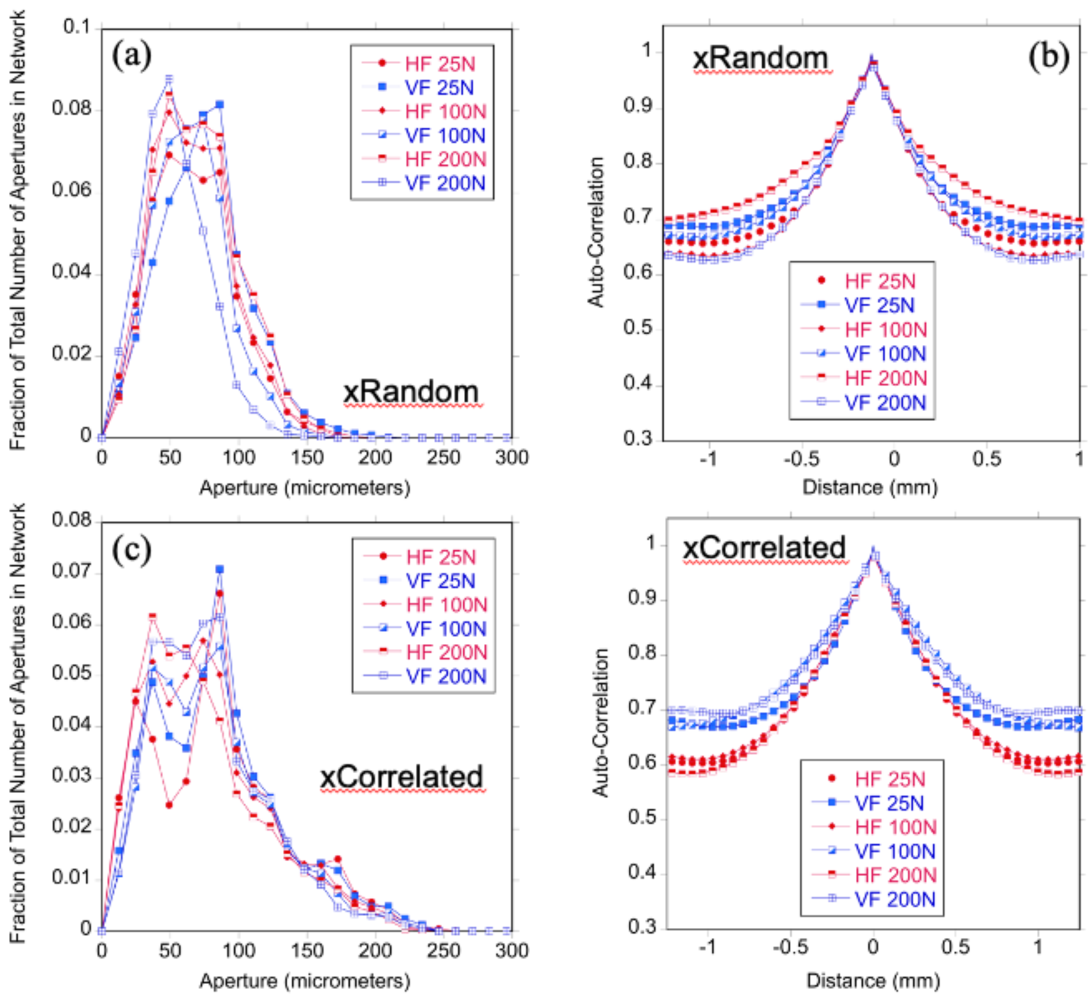

Figure 7. (a&c) Aperture distributions and (b&d) auto-correlation functions for normal loads of 25, 100 and 200 N for (a&b) a random (sample: xRandom) and (c&d) spatially correlated (sample: xCorrelated) initial asperity distributions. HF – horizontal fracture, VF – vertical fracture.

The 3D reconstructions of the elemental fracture intersection topology help to identify the key changes in network connectivity caused by stress. For instance, in the x-configuration, when the intersection and fractures in a network close uniformly, the fractures can disconnect and transition from an "X" to a "V" topology. Thus understanding how connectivity around the corners is affected by the geometry of the individual fractures is crucial for predicting the properties of "corner flow". In the +-configuration, when only one fracture is affected by stress, the connectivity and area fractions of the void spaces differs in each fracture, leading to a mixed percolation regime.

For both configurations, connectivity in the direction along the intersection (i.e. front-to-back (FB)) is controlled by the relative area fractions and connectivity of the void spaces in each of the two fractures as well as along the intersection. For FB flow in the "+" orientation, the vertical fracture controls the connectivity that is enhanced by the intersection that does not close under stress even when the horizontal fracture is only weakly connected front to back (Figure 4). These observations motivated our percolation analysis using Monte Carlo simulations of fracture network connectivity to include: (1) mixed percolation (section 4.2) versus homogeneous percolation (section 4.1) to capture the difference in fracture void geometry as a function of stress for the "+" and "x" orientations, respectively, and (2) examination of percolation around corners to capture the effect of closing an intersection and to understand how spatial correlations carry around corners (sections 4.1.2 & 4.2.2).

3 Percolation & Finite Size Scaling Analysis

In this section, we describe a percolation analysis approach to study finite-size scaling of percolation probabilities as a function of changing area fractions by considering spanning paths: 1) across an intersection (LR), 2) in the direction parallel to the intersection (FB), and 3) around corners (NW) (refer to Figure 8 d&e for nomenclature).

3.1 Network Construction

A stratified percolation approach is used to generate patterns of aperture distributions for the individual fracture planes. Stratified percolation is a correlated percolation model that is a hybrid between a Sierpinski carpet and random continuum percolation that generates correlated aperture distributions with tunable spatial correlation lengths (D. D. Nolte, and Pyrak-Nolte, L. J., 1997; D. D. Nolte & Pyrak-Nolte, 1991; Petrovitch et al., 2014; Pyrak-Nolte et al., 1988). Construction of an aperture distribution starts within the 1st tier (largest scale) where N points (points per tier) are randomly located within the size of the array. Each point defines the center of a set of N second tiers that are reduced in size from the previous tier by a scale factor b. The process is then iterated for a third tier and fourth tier, etc., each time reducing the size of the tier by the scale factor b. Within each final tier, N points are plotted with a selected point size. The accumulating plotted points overlap, and each time a point is placed, the array element at the positions of overlap are incremented by 1 unit of aperture. The resulting fractal geometry of fracture voids depends on the number of tiers n, on the number of points selected per tier N, on the point size and on the scale factor b. The scale factor is calculated as

$$b = \left(\frac{array\ size}{pointsize}\right)^{1/n}. \qquad (1)$$

The construction can stop at any tier. For instance, a single tier (1T) generates an uncorrelated (short-range correlations) percolation pattern (Figure 8a). Selecting two tiers (2T) generates a fracture void pattern that is strongly clumped (mid-range correlations) in area but has relatively uniform apertures within the clumps (Figure 8b), while selecting five tiers (5T) leads to strong long-range correlated void patterns with characteristic log-normal aperture distributions (Figure 8c). Therefore, the stratified model can be tuned nearly continuously from uncorrelated continuum

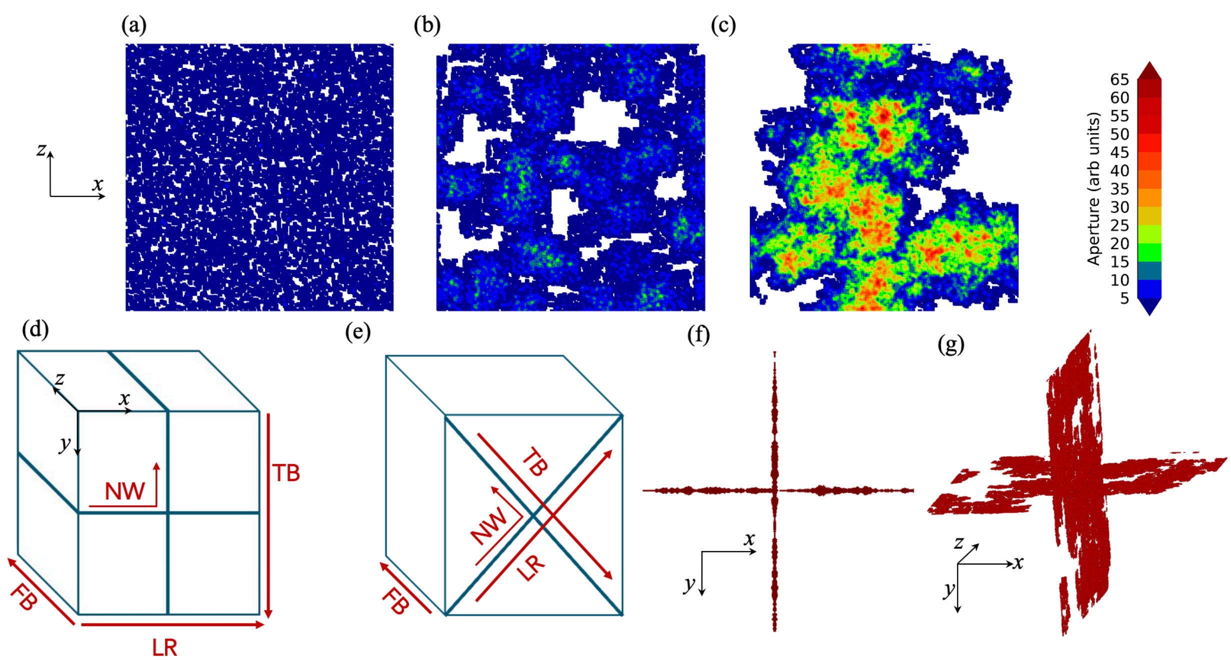

Figure 8. Examples of stratified percolation aperture distributions generated for (a) 1 Tier, (b) 2 Tiers and (c) 5 Tiers. The fracture aperture distribution is inserted into a 3D array to create (d) a "+ or (e) an "x" orientation of the "X" topological element. (f) 2D subsection of a fracture network to illustrate the aperture distribution along the planes and intersection for the same N for both fractures. (g) An example of simulated network with different area fractures for a 5 Tier generation. The connectivity of the network was examined for the directions in shown in (d & e) FB – front to back which is in the direction parallel to the intersection; LR – left to right and TB – top to bottom which cross the intersection, and NW – northwest to probe connectivity around corners.

percolation to strongly correlated continuum percolation with aperture distributions that are multifractal (Pyrak-Nolte et al., 1992).

In this study, we generated aperture distributions for the individual fracture planes that had short- (1T), mid- (2T) and long-range (5T) correlations. Table 1 lists the parameters used to generate the aperture distributions of the fracture planes for the percolation analysis (and to generate the asperity distributions for our fabricated laboratory samples). The number of points per tier were varied in increments (Table 1) to simulate the change in void area fracture as a function of stress. Figure 8 a-c gives examples of 1T, 2T and 5T aperture distributions for an area, $A \sim 0.8$. The 1T and 5T models are representative of the end members of spatial correlations observed in laboratory

Table 1. *Parameters used to generate the asperity patterns for the laboratory samples and aperture distributions for the percolation analysis.*

	Laboratory Random Asperity Distribution	Laboratory Correlated Asperity Distribution	Random or Short-range (1T) Aperture Distribution	Mid-range (2T) Correlated Aperture Distribution	Long Range (5T) Correlated Aperture Distribution
Number of Tiers, *n*	1	3	1	2	5
Points per Tier, *N*, in both Fractures (*“x”*) and in Horizontal Fracture (*“+”*)	5,376	28	90,000-420,000 (increments 30,000 points)	300-1015 (increments of 65 points)	8-19 (increments of 1 point)
Points per Tier, N_v, in the Vertical Fracture for “+”	NA	NA	150,000 210,000 240,000	430 560 755	11 15 19
Point Size, *ps*	5	5	4	4	4
Array Size	180x180	180x180	2060x2060	2060x2060	2060x2060
Number of Networks Single Fracture *“x”* *“+”* *“+”* $A_1/A_2 = 1.0$ *“+”* $A_1/A_2 = 0.8$ *“+”* $A_1/A_2 = 0.75$ *“+”* $A_1/A_2 = 0.6$ *“+”* $A_1/A_2 = 0.5$	 NA	 NA	 100 100 500	 100 100 500 100 100 100 100 100	 500 500 500

samples. 1T is essentially a random distribution often observed in more homogeneous rock (mineralogy, grain size) such as a sandstone or some granites. A 5T model represents fractures that exhibit flow channeling, for example., fractures with heterogeneous mineral distributions that have been preferentially eroded. A 2T model would not be commonly observed in the field because of the patchiness of the void area. However, the 2T model is important because it represents a case intermediate between short- and long-range correlations.

The fracture aperture distributions (e.g. Figure 8a-c) were used to create the void volumes of the fracture network (e.g. Figure 8f). For the "x" orientation condition, two different aperture distributions (i.e. one for each fracture) but with the same statistical properties were generated using the same parameters (Table 1) but with different seeds for the random generator to randomly position the points. The two patterns were statistically similar, but the exact spatial and probabilistic distributions differed. For the "+" orientation conditions, the horizontal fracture was generated for a range of N values to simulate changes caused by stress, and the vertical fracture was generated for a fixed N. The N for the vertical fracture for the "+" condition (Table 1) were chosen to generate area fractions in the vertical fracture that were less than, near and greater than A_c. Patterns for the vertical and horizontal fractures were generated with an array size of 2060 x 2060 pixels from which a 1027 x 1027 array was extracted from the center to avoid any possible edge effects from the creation of the pattern which uses a "wrap-around" approach during creation (see (D. D. Nolte & Pyrak-Nolte, 1991) for more details). After generating the patterns for the vertical and horizontal fractures, a 3D array (1024 x 1024 x 1024 pixels^3) was created and set equal to 0 for all array elements. Then a centered 1024x1024 array was extracted from the fracture aperture patterns to insert into the 3D array to form an "X" topology network as shown in Figures 8f&g. Next the void volume was created by expanding the aperture from the 2D plane into the volume (Figure 8f) on either side of the initial inserted fracture. The matrix on either side of a fracture was eroded based on the value of aperture at that location. For example for the horizontal fracture, if location (i, j) had an aperture = 8 units, then voxels ($i , j, z\text{-}4\text{:}z\text{+}4$) would be set equal to 1. This results in mirrored surfaces similar to that used in the experiments. If an aperture at a location was 0 this represented contact area between the 2 surfaces. For the voxels of intersection between the 2 fractures, the void value of the voxel was taken as the logical OR of the individual void values of the two fractures. Therefore, if either fracture has a void value of 1 at that voxel, then the resulting intersection had a void value of 1. Figure 8g is an example of a *"+"* network, i.e. the fractures have different void area fractions. The number of simulations run for the different conditions are listed in Table 1.

3.2 Stress-Displacement Calibration

Fracture void geometries deform under stress as far-field stresses compress the asperities of the fracture geometry and deform the voids (Hopkins, 1990; Pyrak-Nolte, 2019). The resulting far-field stress-displacement curves of fractures in crystalline rock define an effective parameter of the fracture known as the static *fracture specific stiffness* that can be interpreted approximately as a distribution of springs under compression. In previous work (Pyrak-Nolte et al., 1988), we have shown how to extract the stress-displacement curves from the stratified percolation construction described above. To provide a stress calibration for the model, we consider fractures in granite with specific stiffness of 10 TPa/m with an asymptotic maximum displacement of 5 micrometers (Cook, 1992; Pyrak-Nolte et al., 1987). This spans the number of points per tier in the model construction for 1T from 90,000-420,000, for 2T from 300-1015 and for 5T from 8 to 19. A graph of the calculated stress-displacement is shown in Figure 9a including the specific stiffness (Figure 9b), which is defined as the derivative (tangent slope) of the displacement-stress curve.

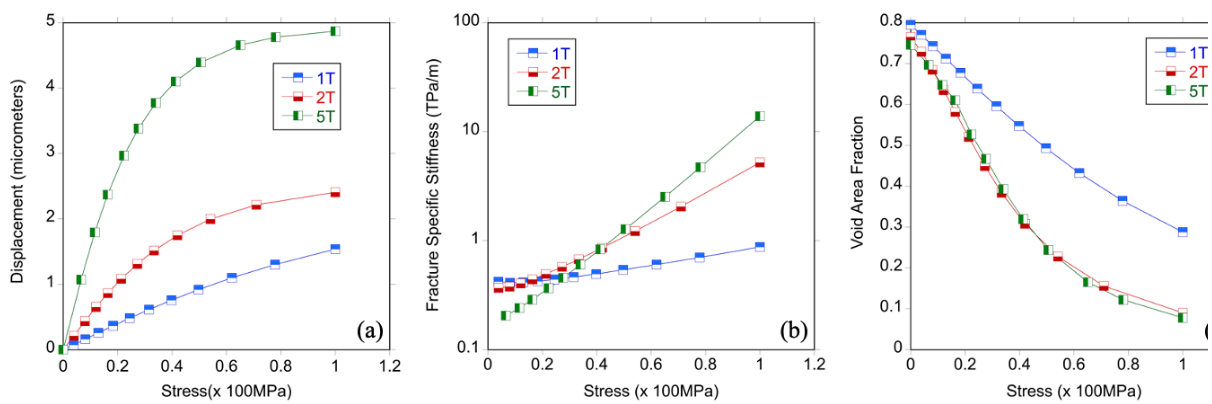

Figure 9. For 1T, 2T and 5T fracture aperture patterns (a) the displacement-stress, (b) fracture specific stiffness-stress and (c) void area fraction versus stress curves.

The key calibration curves for the percolation analysis are shown in Figure 9c. Percolation through two-dimensional fractures is described as a probability for the void geometry to span the fracture, at a given observation scale, as a function of the void area fraction. The relationship between area fraction and stress is nonlinear because of the asymptotic closure of the fracture under high stress. In the following percolation probability graphs, the spanning probability as a function of area fraction can be converted back to fracture specific stiffness and stress for fractures at a selected scale. This calibration sets a nominal fracture stress-strain behavior for meter-scale fractures of 1-10 micrometer average aperture in crystalline rock. Fracture stiffness has been found to follow scaling relations (Petrovitch et al., 2014; Pyrak-Nolte, 2019; Pyrak-Nolte & Nolte, 2016), allowing the stress-displacement properties discussed in the follow sections to be scaled up to larger field sites as well as down to laboratory scales.

3.3 Analysis Approach

Once the simulated "X" topological networks were created, the spanning probability of the network was determined for the directions shown in Figure 8d&e, namely FB, LR, TB and NW. Other corners were studied but produced the same result and are not shown for brevity. A custom function was written in the IDL language to determine if two sides of a sample were connected (LR, TB, FB, NW) after using the "label_region" function to identify connected regions. Then the function found the subscripts of the unique elements on opposing faces (e.g. left and right face for LR, or north and west for NW) and performed a comparison of the elements. If a match occurred, then a percolation cluster existed between the two faces under examination. For the finite-size scaling analysis, the spanning probability is calculated at different scales. This was achieved by sub-sectioning the 3D array into smaller arrays centered around the intersection and sectioned along the intersection. The array edge lengths were 32, 64, 128, 256, 512 and 1024 which resulted in 32, 16, 8, 4, 2, and 1 subsections, respectively, per network. Table 1 lists the number of networks generated at the largest scale so that the average spanning probability was based on total spanning probability at each scale divided by the number of simulations times the number of subsections. The average area fraction, A_{ave}, is based on the area fraction of the fracture that is changing which is approximately the A_{ave} for a single fracture with the same statistics. Spanning probabilities for two parallel fractures used the spanning probabilities of the individual fractures to calculate the spanning probability for two parallel fractures, $P_{||}$, namely

$$P_{||}(A1, A2) = P_1(A1) + P_2(A2) - (P_1(A1) * P_2(A2)). \tag{2}$$

where $P_1(A1)$ and $P_2(A2)$ are the spanning probabilities of the individual fractures as a function of void area fraction. When both fractures have the same statistical properties, equation (2) becomes

$$P_x(A) = 2P(A) - P(A)^2 \qquad (3)$$

where $P(A) = P_1(A) = P_2(A)$. The equation was validated against Monte Carlo simulations of three-dimensional percolation for two independent non-intersecting fractures.

4. Results & Discussion

In this section, we present and discuss the results from the percolation and finite-size scaling analyses, for the x-orientation where both fractures experience the same change in void volume area fraction (homogeneous percolation), and then for the +-orientation where only the void

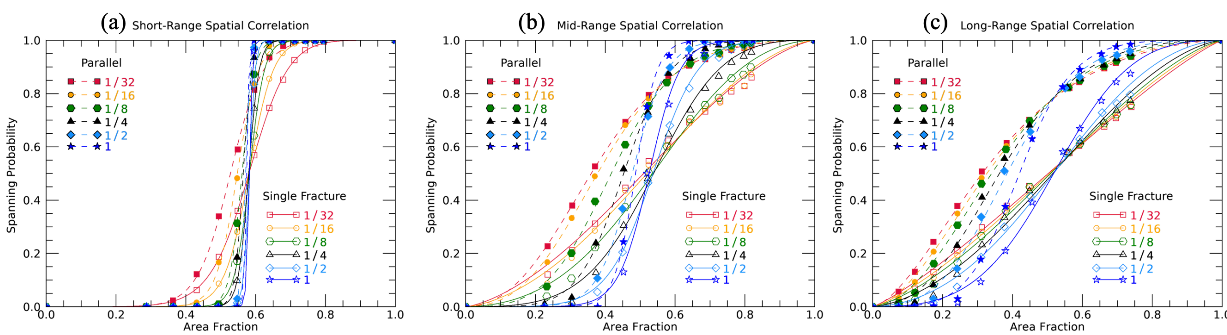

Figure 10 . Comparison of the spanning probability for a single fracture, P_{FB}, (open symbols, solid line) with that for two parallel fractures, $P_{||FB}$, (filled symbols, dashed line) as a function of void area fraction and for observation scales 1/32, 1/16, 1/8, ¼, ½ and 1 for fractures with (a) short-, (b) mid- and (c) long-range spatially correlated aperture distributions.

volume in the horizontal fracture changes with stress (mixed percolation). The final section contains results for conditions between these two limiting cases when both fractures experience different non-zero stresses.

4.1 Connectivity of a Single Fracture vs Parallel Fractures

When moving from a single fracture to a set of parallel fractures, the probability of having a connected path across a sample increases, as shown in a comparison of the spanning probability for a single fracture and two parallel fractures in Figure 10 for aperture distributions with short-, mid- and long-range spatial correlations. The critical area fraction, A_c, for the threshold remains the same for one or a set of parallel (non-intersecting) fractures, but the magnitude of the spanning probability increases with increasing number of parallel fractures because of the multiplicity of possible paths across the sample. As expected, having two statistically similar fractures enhances the probability of having a connected path across a fracture sample for all observations scales.

4.2 Connectivity Front to Back: Comparison of Intersecting Fractures vs Parallel Fractures

A key question is whether two intersecting fractures provide more connectivity and potentially more flow than two parallel fractures. To address this question, we compared the spanning probabilities as a function of scale for two independent parallel fractures relative to the case of two intersecting orthogonal fractures in the FB direction, i.e., in the direction parallel to the long axis of the intersection (see Figure 8e). This is in the same direction as the flow measurements by Stanton-Yonge et al (Stanton-Yonge et al., 2023). For homogeneous percolation (i.e., "x" orientation) with both fractures under the same stress, the average area fractions for both fractures are the same. The additional void volume that is provided by the fracture intersection contributes a positive increment to the percolation probability relative to the two independent (parallel) fractures based on simple mathematical additivity. Therefore, the question is not whether fracture intersections increase connectivity and flow, but by how much?

4.2.1 Homogeneous Percolation: Front-to-Back Connectivity

Figure 11a-c shows the "x" spanning probabilities in the FB direction as a function of void area fraction for aperture distributions with short-, mid- and long-range spatial correlations for the different observation scales. The dependence on area fraction represents the reduction in the apertures and increase in contact area that occurs with increasing stress. Two sets of curves are shown in each subplot. The dashed curves are the percolation probabilities for two independent parallel fractures. The solid curves are the percolation probabilities for the intersecting x-orientation. Both sets of curves exhibit scaling behavior, i.e., there is a fixed point at A_c above which the spanning probability P for a given A decreases with decreasing scale of observations, and below increases with decreasing scale of observations. At the fixed point, A_c, the spanning probability P is scale invariant.

The critical thresholds and the spanning probabilities at the critical thresholds are shown in Fig. 11d. The differences of interest are when considering two independent non-intersecting fractures (i.e., parallel fractures) relative to the equivalent fractures when they are intersecting. For fractures with no correlations other than short range (Figure 11a) the threshold A_c stays approximately unchanged, but the spanning probability at threshold is increased by the intersection. In contrast, when longer-range correlations are present (e.g. 11c and the green open squares in Figure 11d) in the two intersecting fractures, the threshold A_c and the spanning probabilities at threshold are lower than for two parallel fractures. The lower A_c for the intersecting

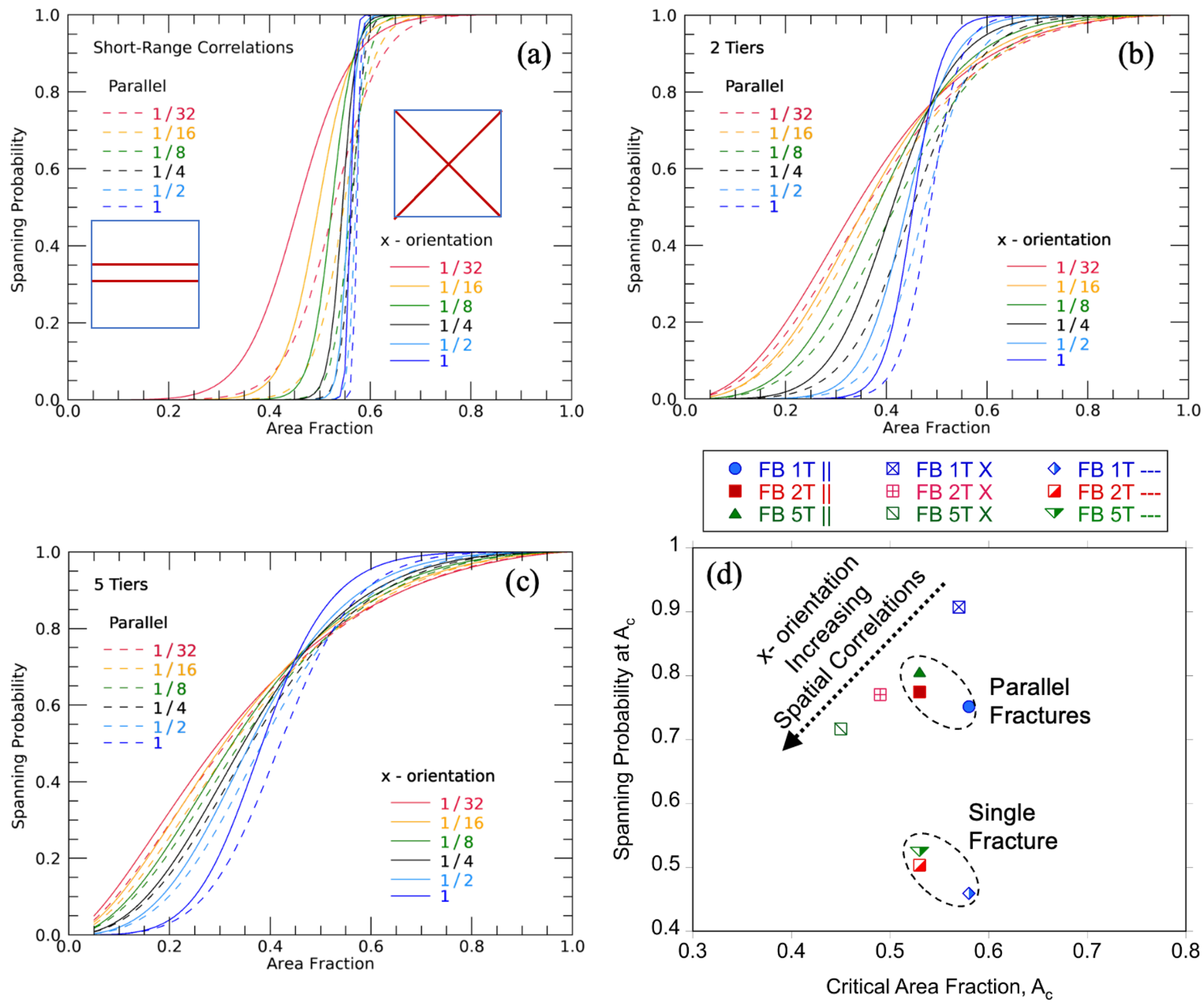

Figure 11. Front-to-back (FB) comparison of the spanning probability for the "x" orientation (homogeneous percolation), P_{xFB}, with that for two parallel fractures, $P_{||FB}$, as a function of void area fraction and for observation scales 1/16, 1/8, ¼, ½ and 1 for fractures with (a) short-, (b) mid- and (c) long-range spatially correlated aperture distributions. (d) A comparison of $P_{xFB}(A_c)$ and $P_{||FB}(A_c)$, i.e. at the fixed point, for the different aperture distributions.

fractures is a consequence of flow paths that can move out of one fracture plane and into another, allowing for an increased number of possible flow paths front-to-back. This increases the options for spanning that lowers the threshold, and fractures can percolate under stresses that would have mostly prevented flow in the individual parallel fractures. The shift in the threshold (i.e., A_c) is approximately 5-10%. This shift would have significant effect on flow for systems that are near their percolation threshold.

4.2.1 Mixed Percolation: Front-to-Back Connectivity

For the "+" FB orientation, only one fracture in a network is subjected to stress, the amount of contact area differs between the two fractures, as does the aperture distribution and the spatial correlations in the two fractures as observed in the laboratory data (Figures 4 & 5). Mixed percolation conditions were created by holding the vertical fracture at a fixed stress, i.e. fixed A. Three stresses were selected to produce void-space connectivity below, near, and above the percolation threshold (see Methods Table 1). Examination of the spanning probability (Figure 12) for aperture distributions with short- , mid- and long-range spatial correlations (Figure 12) show that when $A_v > A_{ch}$, no fixed point exists, $P_{+FB} \sim P_{||FB}$ and larger observation scales exhibit a higher P for all A for spatially correlated aperture distributions (see Figure 12c, f, and i). When $A_v < A_{ch}$, P_{+FB}, $\sim P_{||FB}$, for spatially correlated aperture distributions (see Figure 12d and g). Thus, for $A_v < A_{ch}$ and $A_{ch} < A_v$ the behavior is essentially a 2D connectivity problem. Only when A_v is near A_{ch} does the intersection play an important role in connectivity. The vertical fracture provides additional connectivity creating a 3D connected path rather than just the 2D connectivity of two parallel fractures. This is illustrated in Figure 13 where the horizontal fracture (Figure 13a) and the vertical fracture (Figure 13b) individually are not connected front to back. Both of these patterns would yield a spanning probability of 0 leading to $P_{||FB} = 0$ for two parallel fractures. However, by rotating one fracture by 90 degrees to form an intersection between the two fractures, a connected flow path is formed front to back (Figure 13c). Hence, the intersection enables connectivity through a

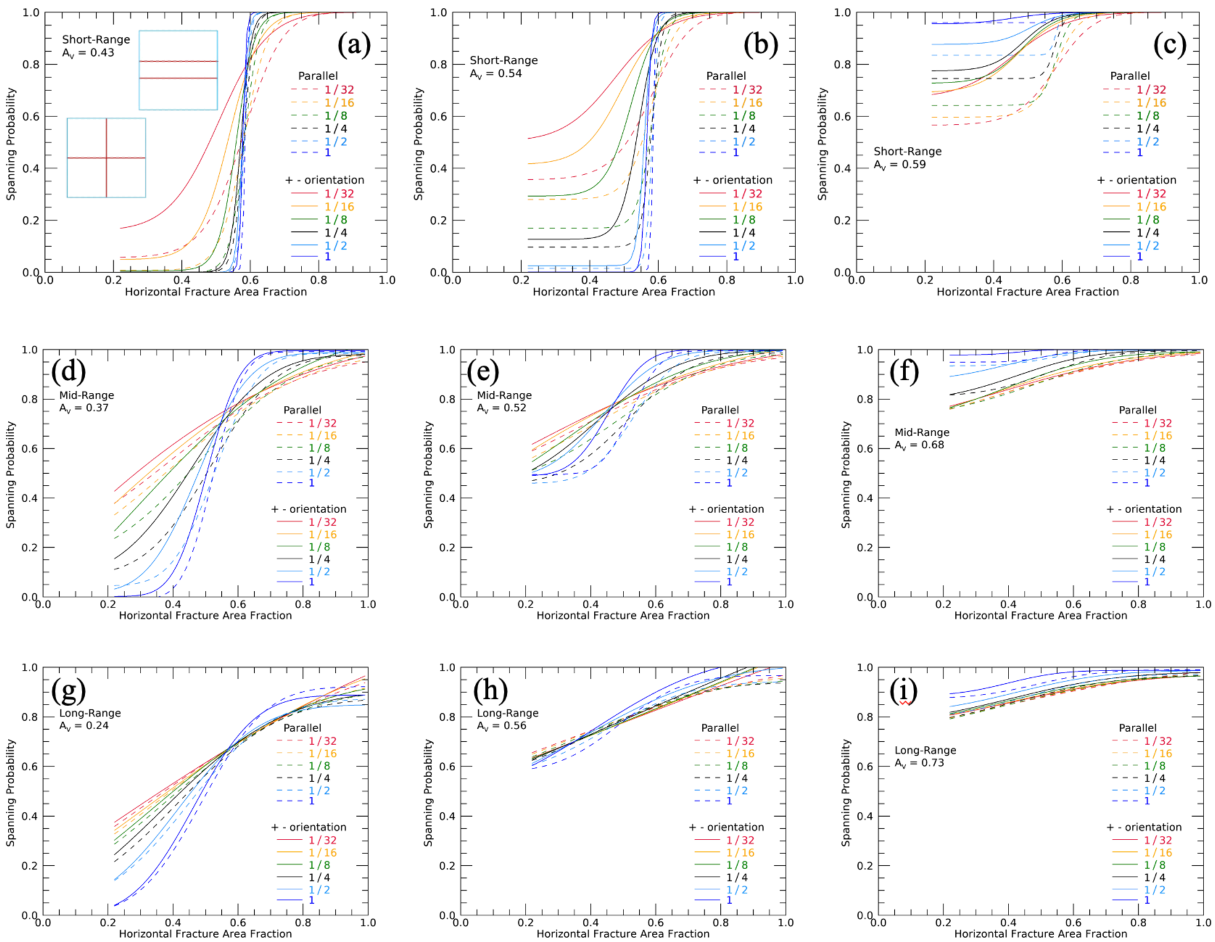

Figure 12. Comparison of the spanning probabilities , P_{FB}, as a function of the horizontal fracture void area fractionfor mixed percolation conditions for 2 parallel fractures versus 2 orthogonal intersecting fractures ("+" orientation) where the area fraction of the vertical fracture, A_V, does not change. (a-c) 1T, (d-f) 2T and (g-i) 5T. The area fraction for the vertical fracture is (left column) below, (middle column) near and (right column) above A_c of the horizontal fracture.

3D tortuous path through both fractures. The connection across the intersection provides a small link to increase the P_{+FB} and to shift the fixed point to a lower A_c than for two parallel fractures.

4.3 *Connectivity across Intersections and around Corners*

Here we examine the effect of intersections on connectivity across intersections (LR) and around corners (NW) for the two cases of "x" homogeneous percolation, where the area fraction of both fractures closes under stress and have the same area fractions, and "+" mixed percolation, where the area fraction only changes in one of the fractures with increasing stress. Because fractures in the field exhibit a range of orientations relative to a stress field, results are also presented for intersection orientations between the "x" and the "+", all of which have mixed percolation except for the "x" limit.

4.3.1 Homogeneous Percolation: "x" orientation

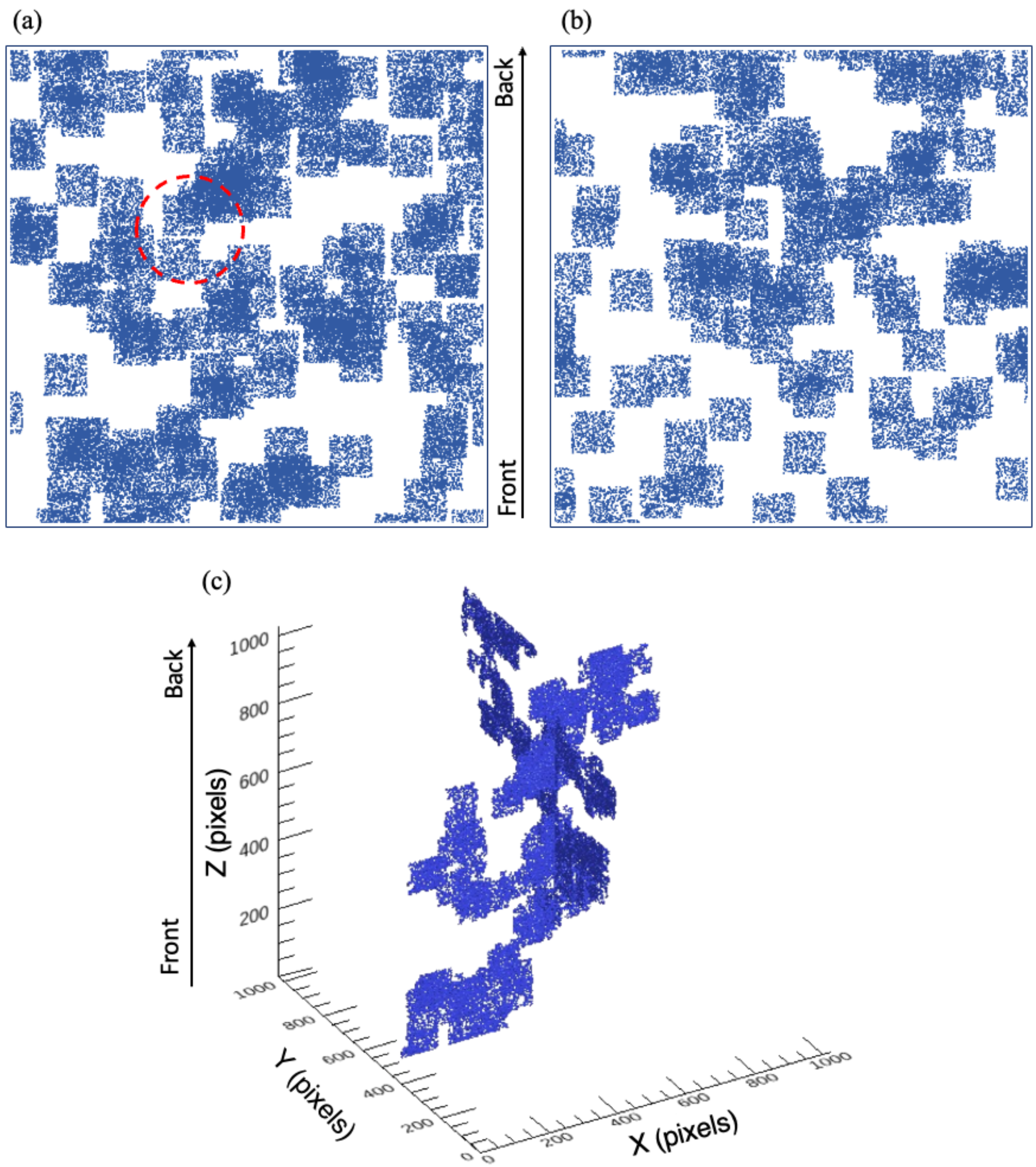

Figure 13. The void distribution in (a) the horizontal and (b) the vertical fracture with mid-range spatially correlated aperture distributions. Note that the individual fractures do not have a connected path from front to back. The dashed red circle highlights the region where the horizontal fracture is not connected front to back. (c) The connected path from front-to-back for two intersecting fractures in the mixed percolation conditions.

When both fractures are subjected to the same stress, the change in void area fraction is the same in both fractures. For statistically similar fractures, this results in similar spanning probabilities for P_{LR} and P_{TB}. For corner percolation, the same P occurs around all 4 corners (NW, NE, SW and SE in Figure 8e). Thus here we only compare P_{LR} to P_{NW} (Figure 14) for the "x" orientation (homogeneous percolation) for different spatial correlations.

In all cases, P_{LR} is larger than or equal to P_{NW}. For short-range correlations (Figure 14a), P_{LR} and P_{NW} are approximately equal. As the range of the correlations increases (from mid- to long range Figures 14b&c), the fixed point for P_{NW} shifts to lower area fractions than for P_{LR} (Figure 14d). At large observation scales (i.e. 512, 1024), P_{LR} and P_{NW} exhibit similar spanning probabilities. However, at smaller observation scales, P_{NW} probabilities are suppressed relative to P_{LR} (e.g. Figure 14c). These trends occur because, although the horizontal and vertical fractures are statistically similar, they were generated using different random seeds. Therefore, all correlations are broken discontinuously around corners. In nature, fractures are not expected to have the same void space distribution though they may have the same void volume because of the details of how the fracture was formed as well as the mineralogy (Jiang et al., 2020), including geochemical alterations that lead to local variations in surface roughness/aperture distribution. The

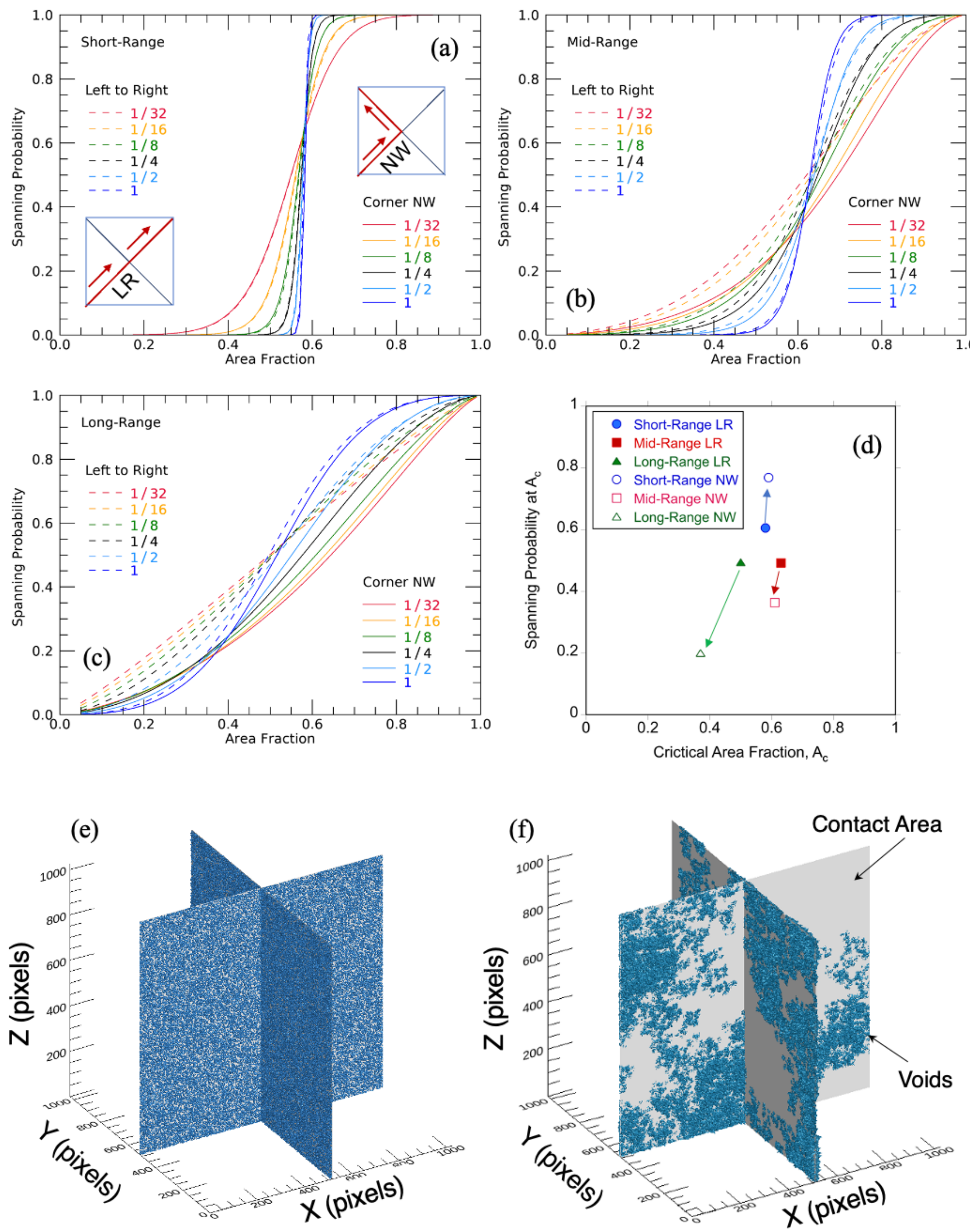

Figure 14. Corner spanning probabilities, P_{xLR} and $P_{x\lrcorner}$, homogeneous percolation, as a function of fracture void area fraction for (a) short-, (b) mid-and (c) long-range spatially correlated aperture distributions as a function of void area fraction and for observation scales of 1/16, 1/8, ¼, ½ and 1. (d) A comparison $P_{xLR}(A_c)$ and $P_{x\lrcorner}$ (A_c), i.e., at the fixed point for "x" fracture configuration for the different aperture distributions.The arrows indicate the shift in P and A_c from P_{xLR} to P_{xNW}. (e) Short-range and (f) long-range correlations intersecting fractures illustrating the effect of spatial corners on connectivity around corners.

discontinuous break causes correlated clusters on one plane to be disconnected from correlated clusters on the other plane (Figure 14f), reducing the spanning probability.

The scale-invariant fixed point for corner flow is affected by spatial correlations in the aperture distribution (Figure 14d). For short-range correlations, the fixed point for P_{LR} and P_{NW} have the same A_c, because the break in the spatial correlation around corners is negligible (Figure 14e). However, when spatial correlations become important, the smaller-scale spanning probabilities are significantly suppressed (Figure 14b&c), shifting the fixed point A_c to lower values (Figure 14d). For instance, the fixed point for P_{NW} for a 5T network occurs at 38% area fraction even as the

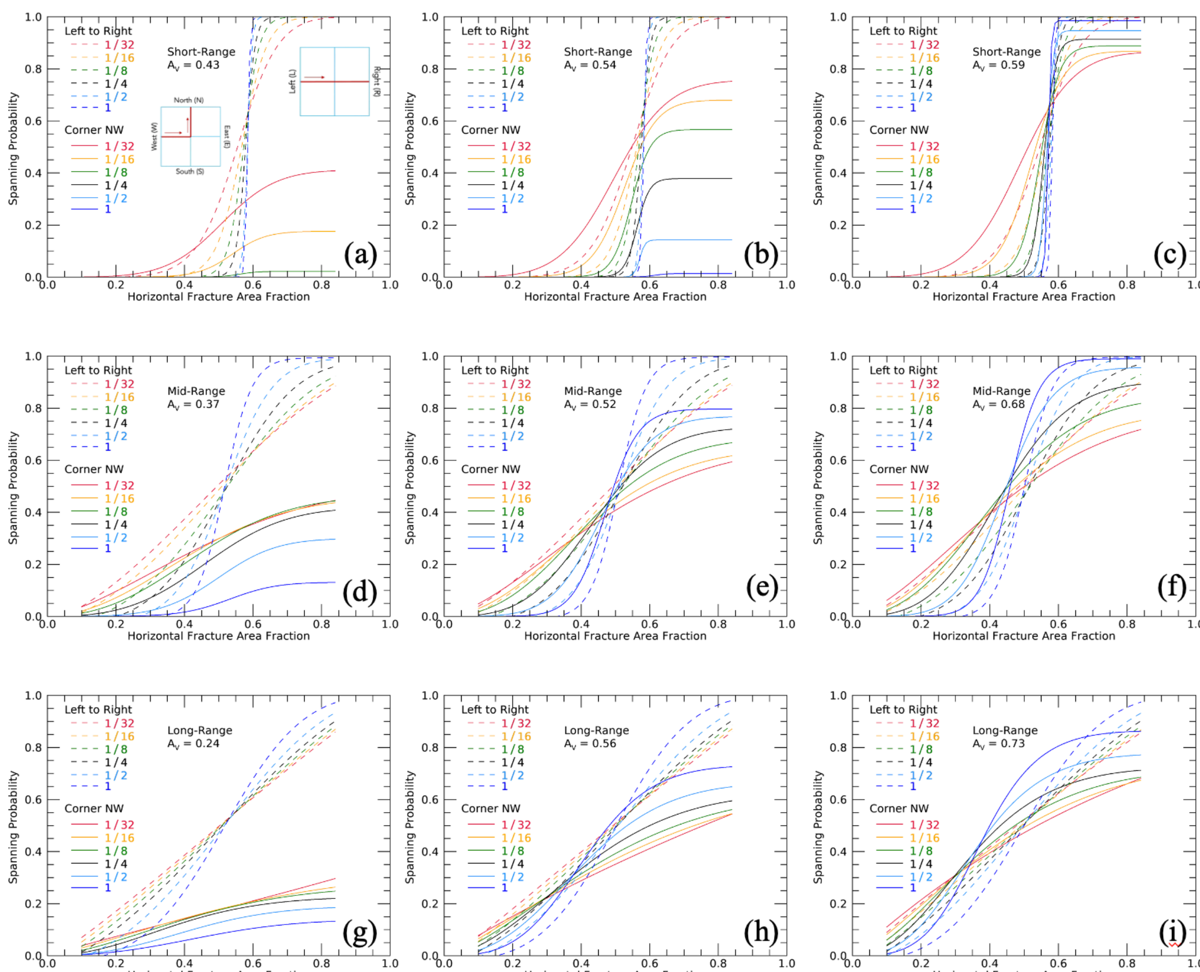

Figure 15. Comparison of the spanning probabilities , P_{LR} and P_{NW} as a function of void area fraction of the horizontal fracture for mixed percolation conditions for 2 parallel fractures versus 2 orthogonal intersecting fractures where the area fraction of the vertical fracture does not change. (a-c) 1T, (d-f) 2T and (g-i) 5T. The area fraction for the vertical fracture is (left column) below, (middle column) near and (right column) above A_c of the horizontal fracture.

probability of having a connected path is less than 20%. P_{NW} has lower values of A_c and $P(A_c)$ relative to the P_{LR} for long-range correlated aperture distributions.

4.3.2 Mixed Percolation "+" orientation

The effects of mixed percolation conditions on P_{+LR} and P_{+NW} when the area of the vertical fraction, A_v, is below, near and above A_c are shown in Figure 15. The rows are short-, mid- and long-range spatial correlations. The columns are by the area fraction of the vertical fracture for A_v which is listed in each graph. Percolation across the horizontal fracture P_{+LR} exhibits scaling behavior and is only minimally affected by A_v with the fixed point shifting at most by a few percent. Unlike for the homogeneous case, P_{+NW} versus A_h is not similar to P_{+LR} (Figure 15). For fractures with the mid- range (Figure 15d) and long-range spatially correlated aperture distributions (Figure 15g), the probability P_{+NW} is *suppressed* relative to P_{+LR} for all scales of observations for $A_h > A_c$, hence the vertical fracture controls the percolation for corner flow. Conversely, for $A_h < A_c$ the probability P_{+NW} is *enhanced* relative to P_{+LR} for all scales of observations because the area fraction $A_v > A_h$, and the vertical fracture contributes higher percolation for corner flow. Therefore, corner flow for mixed percolation in the "+"-configuration is contingent on the fixed properties of the vertical fracture that is not changing with stress. It is either acting as a short (for high A_v) or as an open circuit (for low A_v).

4.3.3 Mixed Percolation for Intermediate Orientations

Intersecting fractures in outcrops and the subsurface will not always be oriented relative to a stress field like the "x" and "+" orientations used in our laboratory study. As the network element is rotated from the "+" to the "x" orientation, the system goes from only one fracture experiencing a normal stress to both fractures experiencing roughly the same magnitude of both a normal and shear stress. Here, we examine the effect of fracture orientations on corner flow (i.e., NW) as the two fractures rotate relative to a vertical stress field, causing the area fractions to vary in both fractures.

To establish a relationship between the two fractures, we assume the area fractions are linearly proportional through $A_1 = fA_2$ where $f < 1$. Therefore, as the average area of the fracture network increases, the A_2 fracture passes through its percolation threshold, Aac_2, before the A_1 fracture passes through A_{ac1}. The spanning probabilities are graphed as a function of average area fraction of the entire network denoted by $A_a = (A_1 + A_2)/2$. This yields equations for the critical threshold for the vertical and horizontal fractures:

$$A_{ac1} = (f+1)/4f$$

$$A_{ac2} = (f+1)/4.$$

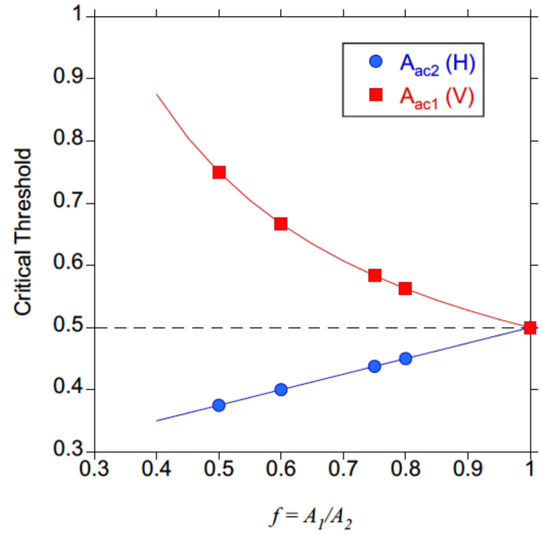

Figure 16. The critical thresholds for the horizontal and vertical fractures as a function of the ratio of their area fractions. The symbols represent the values of the critical threshold for the simulations shown in Figure 17.

Figure 16 shows A_{ac1} and A_{ac2} a function of f from 0.5 to 1.0. When $f = 1$, $A_{ac1} = A_{ac2}$ which represents the "x" orientation. As f decreases, the values of A_{ac1} and A_{ac2} diverge. The divergence of A_{ac1} and A_{ac2} is shown by the dashed lines graphed over the spanning probabilities shown in Figure 17 for different values of f. For corner flow, the two half fractures are in series and thus the spanning probability is dominated by A_1 which has the lower area fraction. Unlike a fixed point where all the curves cross over at a single point, for this mixed percolation, the curves cross through an extended region that is bounded on the high side by A_{ac1} and A_{ac2} on the low side. There are no significant features at A_{ac2}. Below A_{ac2} and above A_{ac1} the scaling behavior is qualitatively similar to homogeneous percolation and the scaling from small to large scales still applies. For example, larger scales having steeper curves continues to be true. But within the cross-over region between A_{ac1} and A_{ac2}, the spanning probabilities are best described by an envelope known as an evolute, for which there is no distinct fixed point. If A_a, the average area of the network, is near threshold, there is no clear scaling for corner flow path connectivity.

5 Discussion and Conclusions

The intersection between two fractures is a basic topological element from which a fracture network system is composed. Furthermore, the effects of the intersection on connectivity across, along or between fractures can determine how well a fracture network can support fluid transport.

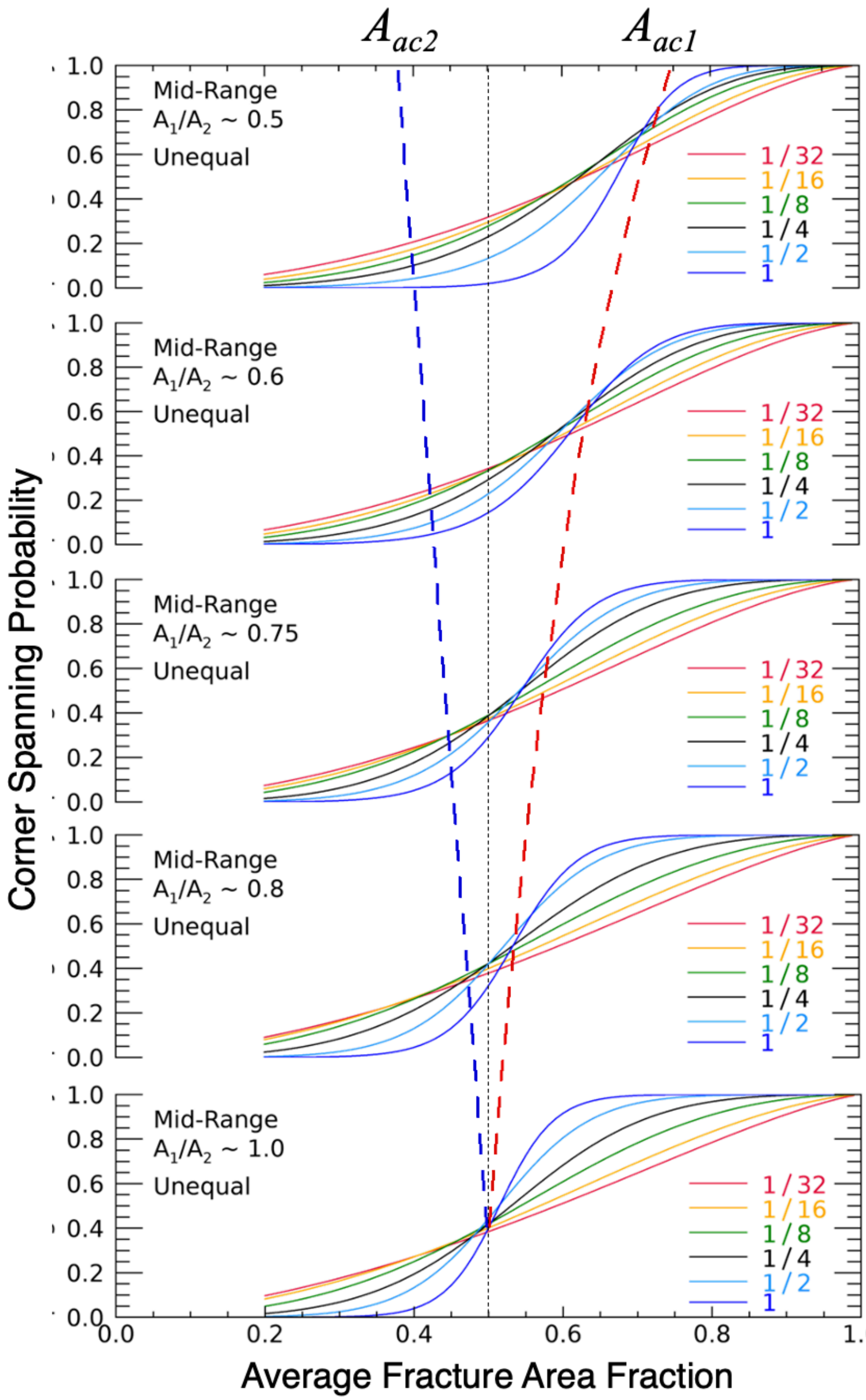

Figure 17. The corner spanning probability as a function of the average network void area fraction for intersecting fractures with mid-range spatial correlations and area fractions that change with stress for $f=A_1/A_2$ (from top to bottom) of 0.5, 0.6, 0.75, 0.8 and 1.0. The dashed curves show the boundaries of the evolute between which no clear scaling behavior exists. The values of the evolute boundaries for the values of f shown here are given by the symbols in Figure 16. The left blue dashed line represents the critical threshold for the A_2 fracture and the right red dashed line represents the critical threshold for the A_1 fracture.

566 for

the understanding of larger fracture networks. By simple additivity, it is clear that an intersection increases connectivity relative to two independent fractures, but what is not as simple is how large the effect on connectivity may be, depending on the properties of the individual fractures and their orientation relative to local stress fields. In some cases, the intersection is fundamental, providing the link from one fracture to another to enable long-range transport through a network. In other cases, the intersection provides little more than an incremental path in parallel with other existing paths. This paper presents a systematic analysis, motivated by 3D x-ray tomography of stressed intersections, of the finite-size scaling of the percolation probabilities of fracture intersections. The results define when intersections play their largest role for which fracture properties and under what conditions.

Whether fracture intersections contribute a large effect to the global connectivity of a fracture network depends on the aperture distributions and their spatial correlations for the individual fractures, including how these properties are altered by stress and by the direction of flow relative to stress. As observed in the laboratory data, stress on a fracture network can reduce the apertures and increase the contact area of the individual planes. Depending on the orientation between the stress field and the fracture system, the intersection is either maintained, or the stress causes the intersection topology to change from "X" to "V". If the fracture properties are related through lithostatic pressure, so that changing stress affects them both equally, then the fracture intersection plays its largest role when the fractures are near their percolation thresholds. The steep slope of the percolation probability near threshold with changing area fraction makes the global connectivity highly sensitive to small changes in local connectivity provided by the fracture intersection. Spanning probabilities can change by factors greater than 2 when comparing the percolation probability of two independent parallel fractures to two intersecting fractures. For instance, when the flow is along the intersection (the FB condition), the intersection in this flow direction acts as a partial short circuit with enhanced front-to-back connectivity, while for flow across the intersection (the LR condition), the intersection has little effect.

In the mixed percolation condition (when only one fracture is subjected to stress), when the flow is along the intersection, the connectivity is dominated by the fracture with the larger area fraction, and again the intersection plays little role. In the "+" configuration, when $A_v > A_h$, then most of the front-to-back connectivity along the intersection is through the vertical fracture, and when $A_v < A_h$, then most of the connectivity is through the horizontal fracture. Only when $A_v \approx A_h \approx A_c$ near the percolation threshold does the intersection contribute significantly to connectivity, as we saw for the homogeneous case.

The situation is very different for corner flow, which takes place only because of the fracture intersection. Without the intersection, there is obviously no corner flow. Furthermore, the local in-plane correlations of the two intersecting fractures change discontinuously around the corner. The break in local correlation reduces connectivity, suppressing the spanning probability. Therefore, fracture intersections act to *suppress* flow relative to the flow through individual fractures with the same properties. This corner flow suppression is strongest for mid-range correlations (2T) because the percolation clusters do not perfectly connect around the corner. For the other two cases of only local short-range correlations (1T) and long-range correlations (5T), the intersection can enhance connectivity. As with flow along the intersection, this enhancement/suppression effect around corners is largest when the fractures are near their percolation threshold. Therefore, while the intersection often acts to enhance flow, there are limited regimes where the intersection can actually suppress flow, keeping in mind that this is always relative to the flow through individual fractures with identical statistical properties, although clearly, in all cases, corner flow does not occur without the intersection.

Therefore, based on this study, the question whether intersecting fractures, natural or induced, enhance the connectivity of a fracture network depends on whether a fracture network is in the homogeneous or mixed percolation regime, and if the void area fractions of the fractures are near, or far, from their critical area thresholds. The rock type would influence the geometry of the fracture surfaces and in turn the aperture distribution. For example, the roughness of fracture surfaces is intimately related to the grain size of the rock, to structural features such as layering and/or an oriented mineral fabric(Jiang et al., 2020), and to geochemical alterations as well as the orientation of an induced fracture with respect to oriented structural/fabric features. In addition, the local stress field affects the amount of void space area available for fluid flow (i.e., A_c) and whether stress is partitioned into normal and shear components. Stress fields are affected by local topography, the presence and orientation of faults and fractures, heterogeneity in physical properties, and depth. For example, a field study (Haimson, 1978) found that the principal horizontal stress was greater than the vertical stress for depths between 20 to 240 m in a quartzite unit in Waterloo, Wisconsin. They observed that the orientation and magnitude of the principal horizontal stresses differed for rocks above and below 20 m which was attributed to surface topography. Thus, fractures in the subsurface are expected to fall more into the mixed percolation regime.

Therefore, achieving homogeneous percolation in nature is expected to be more difficult than in the laboratory. In the laboratory, equal stresses on two fractures was achieved by orienting the network at 45^{o} to the principal stress (i.e., uniaxial load) which resulted in equal partitioning of normal and shear stresses on all fracture planes. In nature, fractures in a network have different orientations relative to the local stress field and/or stress field at the time of formation. Intersecting fractures can occur from a single deformation event that gives rise to multiple fractures or from subsequent events where the stress field between fracture events has changed (Peacock et al., 2018). Once formed, the fractures also affect the local stress field which in turn affects the fracture propagation path and the final void space geometry. Purely lithostatic stress conditions, where the stress is equal in all directions, is a theoretical ideal that is only observable under specific conditions (i.e. minimal tectonic forces, specific range of depths, specific rock type, fluid pressures, etc.). Lithostatic stresses in the Earth's upper crust (0-10km) are often accompanied by a deviatoric stress from the local tectonic environment or other physical processes. Therefore, all of these reasons suggest that the condition of mixed percolation in the field would be significantly more common than homogeneous percolation.

Percolation and finite-size scaling analysis enables the examination of the expected behavior when changing the scale of observations, for example, understanding how laboratory results on the core scale would translate to the borehole scale and potentially reservoir scale. Here, the analysis showed that connectivity around corners breaks scaling particularly when the two fractures in the network are subjected to different stresses, i.e., in the mixed percolation regime. The analysis of mixed percolation when the fractures are subjected to different stresses showed that there is no clear scaling behavior for area fractions between the different thresholds of the two fractures. This raises the question as to whether the ability to scale network behavior is possible in real systems, a question that requires further research.

One of the outstanding open issues is how close or how far the void area fraction of fractures in the subsurface or outcrops are from percolation thresholds. Note that when the average area fraction of the network is below the lower critical threshold (A_{ac1} in Figures 16 & 17) and above the higher critical threshold (A_{ac2} in Figures 16 & 17), traditional scaling behavior still applies. That is, below A_{ac1}, small observations scale have a higher probability of having a connected path than larger scales, and conversely above A_{ac2}, large scales of observation have higher spanning probability than smaller observation scales. These regimes of size-dependent scaling prevent the adoption of representative volumes (REV) for effective medium theory. On the other hand, for very high area fractions near unity, the spanning probability saturates, and effective medium theory does become applicable. Our results suggest that void area fractions greater than about 80% would allow this effective medium approach, for instance for some subsurface applications where increased fluid pressures are used to keep fractures open. However, even if the area fractions on the individual fracture planes are near 80% with spanning probabilities near P = 90%, connecting several of these fractures in series would decrease the probability of having connected path by P^n where n is the number of fractures connected in series.

In conclusion, fracture intersections provide the fundamental link a between fractures within a larger fracture network. If two fractures are near their percolation thresholds, then their intersection adds significant connectivity between the fractures, which enhances long-range transport of fluids. If stresses on the fractures are equivalent, then a homogeneous percolation condition is present, and scale-independent behavior is observed at the critical percolation threshold, which would allow scaling to arbitrary sizes. However, under any mixed percolation condition, which is likely to be the most common case encountered in either the lab or the field, there is strictly no scale-independent spanning probability. This is true for corner flow under any imbalance of stresses. Furthermore, for mid-range correlations, the connectivity around the corner can be lower than expected because of the discontinuous break in correlations going from one fracture to the other. This effect was previously unanticipated and would need to be incorporated in large-scale models of fracture networks. On the other hand, even in the absence of scale-independent behavior near threshold, scale-dependent effects can still be predicted and extrapolated to larger field and smaller lab scales.

Acknowledgments

The authors have no real or perceived financial conflicts of interests.

The work was supported by the U.S. Department of Energy, Office of Science, Office of Basic Energy Sciences, Geosciences Research Program under Award Number (DE-SC0001048).

Open Research

The laboratory data, Monte Carlo data and IDL codes have been deposited on Zenodo with DOI: 10.5281/zenodo.17138336 (Pyrak-Nolte & Nolte, 2025).

References

Asahina, D., Houseworth, J. E., Birkholzer, J. T., Rutqvist, J., & Bolander, J. E. (2014). Hydro-mechanical model for wetting/drying and fracture development in geomaterials. *Computers & Geosciences, 65*, 13-23.

Bai, T. X., Pollard, D. D., & Gao, H. (2000). Explanation for fracture spacing in layered materials. *Nature, 403*(17 February 2000), 753-756.

Berkowitz, B. (2002). Charaterizing flow and transport in fractured geological media: A review. *Advances in Water Resources, 25*, 861-884.

Boutt, D. F., Grasselli, G., Fredrich, J. T., Cook, B. K., & Williams, J. R. (2006). Trapping zones: The effect of fracture roughness on the directional anisotropy of fluid flow and colloid transport in a single fracture. *Geophysical Research Letters, 33*(21). <Go to ISI>://000241865700003

Brown, S., Caprihan, A., & Hardy, R. (1998). Experimental observation of fluid flow channels in a single fracture. *Journal of Geophysical Research, 103*(B3), 5125-5132.

Cook, N. G. W. (1992). Natural joints in rock: Mechanical, hydraulic, and seismic behavior and properties under normal stress. *International Journal of Rock Mechanics and Mining Sciences, 29*, 198-223.

Council, N. R. (1996). *Rock Fractures and Fluid Flow: Contemporary Understanding and Applications*. Washington, D.C.

de Dreuzy, J. R., Davy, P., & Bour, O. (2001). Hydraulic properties of two-dimensional random fracture networks following a power law length distribution: 1. Effective connectivity. *Water Resources Research, 37*(8), 2065-2078.

de Dreuzy, J. R., Meheust, Y., & Pichot, G. (2012). Influence of fracture scale heterogeneity on the flow properties of three-dimensional discrete fracture networks (DFN). *Journal of Geophysical Research-Solid Earth, 117*. <Go to ISI>://WOS:000311257200002

Deng, Q., Schmittbuhl, J., Cacace, M., & Blöcher, G. (2024). Mechanical stiffness and permeability of a reservoir-scale rough fracture during closure. *Journal of Geophysical Research: Solid Earth, 129*(9), e2024JB029001.

Durham, W. B., & Bonner, B. P. (1995). *Closure and fluid flow in discrete fractures.* Paper presented at the *Fractured and Jointed Rock Masses*.

Frampton, A., Hyman, J., & Zou, L. (2019). Advective transport in discrete fracture networks with connected and disconnected textures representing internal aperture variability. *Water Resources Research, 55*(7), 5487-5501.

Frash, L. P., Carey, J. W., Ickes, T., & Viswanathan, H. S. (2017). Caprock integrity susceptibility to permeable fracture creation. *International Journal of Greenhouse Gas Control, 64*, 60-72.

Frash, L. P., Carey, J. W., Lei, Z., Rougier, E., Ickes, T., & Viswanathan, H. S. (2016). High-stress triaxial direct-shear fracturing of Utica shale and in situ X-ray microtomography with permeability measurement. *Journal of Geophysical Research: Solid Earth, 121*(7), 5493-5508.

Frash, L. P., Carey, J. W., & Welch, N. J. (2019). Scalable en echelon shear-fracture aperture-roughness mechanism: Theory, validation, and implications. *Journal of Geophysical Research: Solid Earth, 124*(1), 957-977.

Haimson, B. (1978). *Near-Surface and Deeper Hydrofracturing Stress Measurements in Waterloo Quartzite.* Paper presented at the Transactions-American Geophysical Union.

Hamzehpour, H., Pazoki, S., Khazaei, M., & Sahimi, M. (2021). Dependence of percolation and flow properties of fracture networks on the morphology. *Physica A: Statistical Mechanics and its Applications, 584*, 126361.

He, X., Yu, P., Eijsink, A., Marone, C., Shokouhi, P., Rivière, J., et al. (2025). Co-evolution of specific stiffness and permeability of rock fractures offset in shear. *Journal of Geophysical Research: Solid Earth, 130*(5), e2024JB030633.

Hopkins, D. L. (1990). *The Effect of Surface Roughness on Joint Stiffness, Aperture and Acoustic Wave Propagation.* (Ph.D.), University of California, Berkeley, Berkeley.

Hull, L. C., & Koslow, K. N. (1986). Streamline routing through fracture junctions. *Water Resources Research, 22*(12), 1731-1734.

Jiang, L., Yoon, H., Bobet, A., & Pyrak-Nolte, L. J. (2020). Mineral Fabric as a Hidden Variable in Fracture Formation in Layered Media. *Scientific Reports, 10*(1), 2260.

Johnson, J., & Brown, S. (2001). Experimental mixing variability in intersecting natural fractures. *Geophysical Research Letters, 28*(22), 4303-4306. <Go to ISI>://000172032400038

Johnson, J., Brown, S., & Stockman, H. (2006). Fluid flow and mixing in rough-walled fracture intersections. *Journal of Geophysical Research-Solid Earth, 111*(B12), 16. Article. <Go to ISI>://WOS:000243109400002

Laubach, S. E., Lamarche, J., Gauthier, B. D., Dunne, W. M., & Sanderson, D. J. (2018). Spatial arrangement of faults and opening-mode fractures. *Journal Of Structural Geology, 108*, 2-15.

Laubach, S. E., Lander, R. H., Criscenti, L. J., Anovitz, L. M., Urai, J., Pollyead, R., et al. (2019). The role of chemistry in fracture pattern development and opportunities to advance interpretations of geological materials. *Reviews of Geophysics, 57*(3), 1065-1111.

Montemagno, C. D., & Pyrak-Nolte, L. J. (1999). Fracture network versus single fractures: Measurement of fracture geometry with X-ray tomography. *Physics and Chemistry of the Earth Part a-Solid Earth and Geodesy, 24*(7), 575-579. <Go to ISI>://000082526700004

Mourzenko, V., Thovert, J.-F., & Adler, P. (2005). Percolation of three-dimensional fracture networks with power-law size distribution. *Physical Review E—Statistical, Nonlinear, and Soft Matter Physics, 72*(3), 036103.

Nemoto, K., Watanabe, N., Hirano, N., & Tsuchiya, N. (2009). Direct measurement of contact area and stress dependence of anisotropic flow through rock fracture with heterogeneous aperture distribution. *Earth and Planetary Science Letters, 281*, 81-87.

Nolte, D. D., and Pyrak-Nolte, L. J. (1997). Coexisting two-phase flow in correlated two-dimensional percolation. *Physical Review E, 56*(5), 5009-5012. <Go to ISI>://A1997YH16700021

Nolte, D. D., & Pyrak-Nolte, L. J. (1991). Stratified Continuum Percolation - Scaling Geometry of Hierarchical Cascades. *Physical Review A, 44*(10), 6320-6333. <Go to ISI>://A1991GR73800021

Nolte, D. D., Pyrak-Nolte, L. J., and Cook, N. G. W. (1989). The Fractal Geometry of Flow Paths in Natural Fractures in Rock and the Approach to Percolation. *Pure and Applied Geophysics, 131*(1-2), 111-138. <Go to ISI>://A1989AG51200007

Peacock, A., Sanderson, D. J., & Rotevatn, A. (2018). Relationship between fractures. *Journal Of Structural Geology, 106*, 41-53.

Petrovitch, C. L., Pyrak-Nolte, L. J., & Nolte, D. D. (2014). Combined scaling of fluid flow and seismic stiffness in single fractures. *Rock Mechanics And Rock Engineering*.

Pyrak-Nolte, L. J. (2019). Chapter 14. Fracture specifci stiffness: the critical link between the scaling behavior of hydro-mechanical coupling in fractures and seismci monitoring. In P. Newell & A. Ilgen (Eds.), *Science of Carbon Storage in Deep Saline Formations: Process Coupling Across Time and Spatial Scales"* (pp. 233-251): Elsevier.

Pyrak-Nolte, L. J., Cook, N. G. W., & Nolte, D. D. (1988). Fluid Percolation through Single Fractures. *Geophysical Research Letters, 15*(11), 1247-1250. <Go to ISI>://A1988Q473200019

Pyrak-Nolte, L. J., Myer, L. R., & Cook, N. G. W. (1990). Transmission of Seismic-Waves across Single Natural Fractures. *Journal of Geophysical Research-Solid Earth and Planets, 95*(B6), 8617-8638. <Go to ISI>://A1990DK70100021

Pyrak-Nolte, L. J., Myer, L. R., Cook, N. G. W., & Witherspoon, P. A. (1987). *Hydraulic and Mechanical Properties of Natural Fractures in Low Permeability Rock.* Paper presented at the *Sixth International Congress on Rock Mechanics*, Montreal, Canada.

Pyrak-Nolte, L. J., Myer, L. R., & Nolte, D. D. (1992). Fractures - Finite-Size-Scaling and Multifractals. *Pure and Applied Geophysics, 138*(4), 679-706. <Go to ISI>://A1992LQ89100009

Pyrak-Nolte, L. J., & Nolte, D. D. (2016). Approaching a universal scaling relationship between fracture stiffness and fluid flow. *Nature Communications, 7*, Article Number 10663.

Pyrak-Nolte, L. J., & Nolte, D. D. (2025). Data and Codes for Role of Intersections in Fracture Connectivity. *[Datsets and Software] Zenodo DOI: 10.5281/zenodo.17138336*.

Raven, K. G., & Gale, J. E. (1985). Water flow in a natural rock fracture as a function of stress and sample size. *International Journal of Rock Mechanics and Mining Sciences, 22*(4), 251-261.

Sanderson, D. J., & Nixon, C. W. (2015). The use of topology in fracture network characterization. *Journal Of Structural Geology, 72*, 55-66.

Sanderson, D. J., & Nixon, C. W. (2018). Topology, connectivity and percolation in fracture networks. *Journal Of Structural Geology, 115*, 167-177.

Santos, A. M., Hu, M., & Pyrak-Nolte, L. J. (2022). *Exploring the geometry of fracture intersections*. Paper presented at the 56th US Rock Mechanics/Geomechanics Symposium, Sante Fe, New Mexico.

Stanton-Yonge, A., Mitchell, T. M., & Meredith, P. G. (2023). The Hydro-Mechanical Properties of Fracture Intersections: Pressure-Dependant Permeability and Effective Stress Law. *Journal of Geophysical Research-Solid Earth, 128*(2). <Go to ISI>://WOS:000933220000001

Stauffer, D. (1987). *Introduction to Percolation Theory*. Bristol: Taylor and Francis.

Stockman, H. W., Johnson, J., & Brown, S. R. (2001). Mixing at fracture intersections: influence of channel geometry and the Reynolds and Peclet numbers. *Geophysical Research Letters, 28*(22), 4299-4302. <Go to ISI>://000172032400037

Thovert, J.-F., Mourzenko, V. V., & Adler, P. (2017). Percolation in three-dimensional fracture networks for arbitrary size and shape distributions. *Physical Review E, 95*(4), 042112.

Tirrell, M., Hubbard, S., & Sholl, D. (2017). *Basic Research Needs for Energy and Water* Retrieved from U.S. Department of Energy, Office of Science:

Tsang, C. F., & Neretnieks, I. (1998). Flow channeling in heterogeneous fractured rocks. *Reviews of Geophysics, 36*(2), 275-298.

Tsang, Y. W., & Tsang, C. F. (1987). Channel model of flow through fractured media. *Water Resources Research, 23*, 467.

Viswanathan, H. S., Ajo-Franklin, J., Birkholzer, J. T., Carey, J. W., Guglielmi, Y., Hyman, J. D., et al. (2022). From Fluid Flow to Coupled Processes in Fractured Rock: Recent Advances and New Frontiers. *Reviews of Geophysics, 60*(1). <Go to ISI>://WOS:000777485900006

Welch, N. J., Carey, J. W., Frash, L. P., Hyman, J. D., Hicks, W., Meng, M., et al. (2021). Effect of shear displacement and stress changes on fracture hydraulic aperture and flow anisotropy. *Transport in Porous Media*, 1-31.

Witherspoon, P. A., Wang, J. S., Iwai, K., & Gale, J. E. (1980). Validity of cubic law for fluid flow in a deformable rock fracture. *Water Resources Research, 16*(6), 1016-1024.

Wood, C. E. (2024). *Imaging Elastodynamic and Hydraulic Properties of Fractured Rock: Exploring Effects of Dynamic Stressing, Shearing, Fracture Aperture, and Roughness*: The Pennsylvania State University.

Ye, Z., Fan, X., Zhang, J., Sheng, J., Chen, Y., Fan, Q., & Qin, H. (2021). Evaluation of connectivity characteristics on the permeability of two-dimensional fracture networks using geological entropy. *Water Resources Research, 57*(10), e2020WR029289.